Journal of Structural Geology 141 (2020) 104219

Contents lists available at ScienceDirect

Journal of Structural Geology

journal homepage: http://www.elsevier.com/locate/jsg

Interaction of deformation bands and fractures during progressive strain in monocline - San Rafael Swell, Central Utah, USA

Alvar Braathen [a,*], Elizabeth Petrie [b], Tonje Nystuen [a], Anja Sundal [a], Elin Skurtveit [a,c], Valentin Zuchuat [a], Marte Gutierrez [d], Ivar Midtkandal [a]

[a] Tectonostratigraphic Research Group, Department of Geosciences, University of Oslo, P.O. Box 1047, Blindern, 0316, Oslo, Norway
[b] Natural & Environmental Science Department, Western Colorado University, 1 Western Way, Gunnison, CO, 81231, USA
[c] Norwegian Geotechnical Institute (NGI), P.O. Box. 3930 Ullevål Stadion, N-0806, Oslo, Norway
[d] Department of Civil and Environmental Engineering, Colorado School of Mines, 1610 Illinois St., Golden, CO, 80401, USA

ARTICLE INFO

Keywords:
Deformation bands
Fractures
Monocline
Fold
Laramide orogeny
Utah

ABSTRACT

Folds in porous sandstone in cases allow identification of progressive deformation in an evolving strain field. In the Navajo Sandstone of the km-scale Laramide-style monocline of the San Rafael Swell (Utah, USA), four populations of small-scale structures record different kinematics and deformation mechanisms, depending on orientation to bedding within the first-order fold. Small-scale structures span from cataclastic (shear-) compaction and shear-isochoric deformation bands to dominant disaggregation (shear-) dilation bands. Extension and shear fractures record transformations from band to fracture formation, adding to the structural diversity.

Early structures record semi-penetrative shear deformation guided by bedding and lamination in eolian deposits, consistent with layer-parallel shortening. Subsequent deformation is localized and at a higher angle relative to bedding, recording forward-directed and subsequently backward-directed shear structures within the east-verging monocline. Final deformation is highly localized and appears as a conjugate set of sub-vertical shear zones with shortening-extension axes oblique to the monocline.

For the given conditions in a progressive shear system in highly porous sandstones, interactions of deformation bands and fractures suggest a revival of deformation bands by mutual shear band-fracture systems as developing band swarms rotate into an extensional strain sector during folding. In cases of deformation by shear-dilation strain, deformation bands may evolve directly into fractures, as grain contacts are lost.

1. Introduction

Continuous deformation by folding causes progressive strain in rocks, and folds should accordingly allow study of evolving strain fields if structures from progressive, superimposed stages can be identified. In porous rocks such as sandstone, signatures of evolving deformation may vary, covering compaction seen as collapse of pore space by deformation bands and/or dilation leading to formation of other types of deformation bands or fractures. Theoretically, and especially considering the velocity field in tri-shear kinematic models of fault-propagation folds (e.g., Erslev 1991; Allmendinger 1998; Cardozo and Aanonsen 2009; Cardozo et al., 2011), a multitude of structures may be expected in highly porous rocks. They could span from deformation bands, with shear or pure compaction, to dilational bands, shear fractures and joints (Fig. 1), depending on rock properties and enveloping stresses influenced by fluid pressure. The orientation of structures with respect to the principal strain axes at the stage of formation, with orientations gradually changing with folding, may also play a role. As of today, studies analysing progressive strain-kinematics during continuous deformation mainly target fracture systems, partly addressing deformation mechanisms (Ismat and Mitra 2005; Aydin et al., 2006), but more commonly the importance for fluid mobility (Hancock 1985; Silliphant et al., 2002; Bergbauer and Pollard 2004; Fischer and Christensen 2004). This may be because progressive stages of deformation seldom are readily identifiable. Studies of interlinked folding and deformation band formation are rare (Davis 1999; Cashman and Cashman 2000; Cooper et al., 2006; Wibberley et al., 2008; Zuluaga et al., 2014). This case study unravels the importance of evolving strain in highly porous sandstones during folding, as

* Corresponding author. Department of Geosciences, University of Oslo, Norway.
E-mail address: alvar.braathen@geo.uio.no (A. Braathen).

https://doi.org/10.1016/j.jsg.2020.104219
Received 30 June 2020; Received in revised form 21 October 2020; Accepted 28 October 2020
Available online 1 November 2020

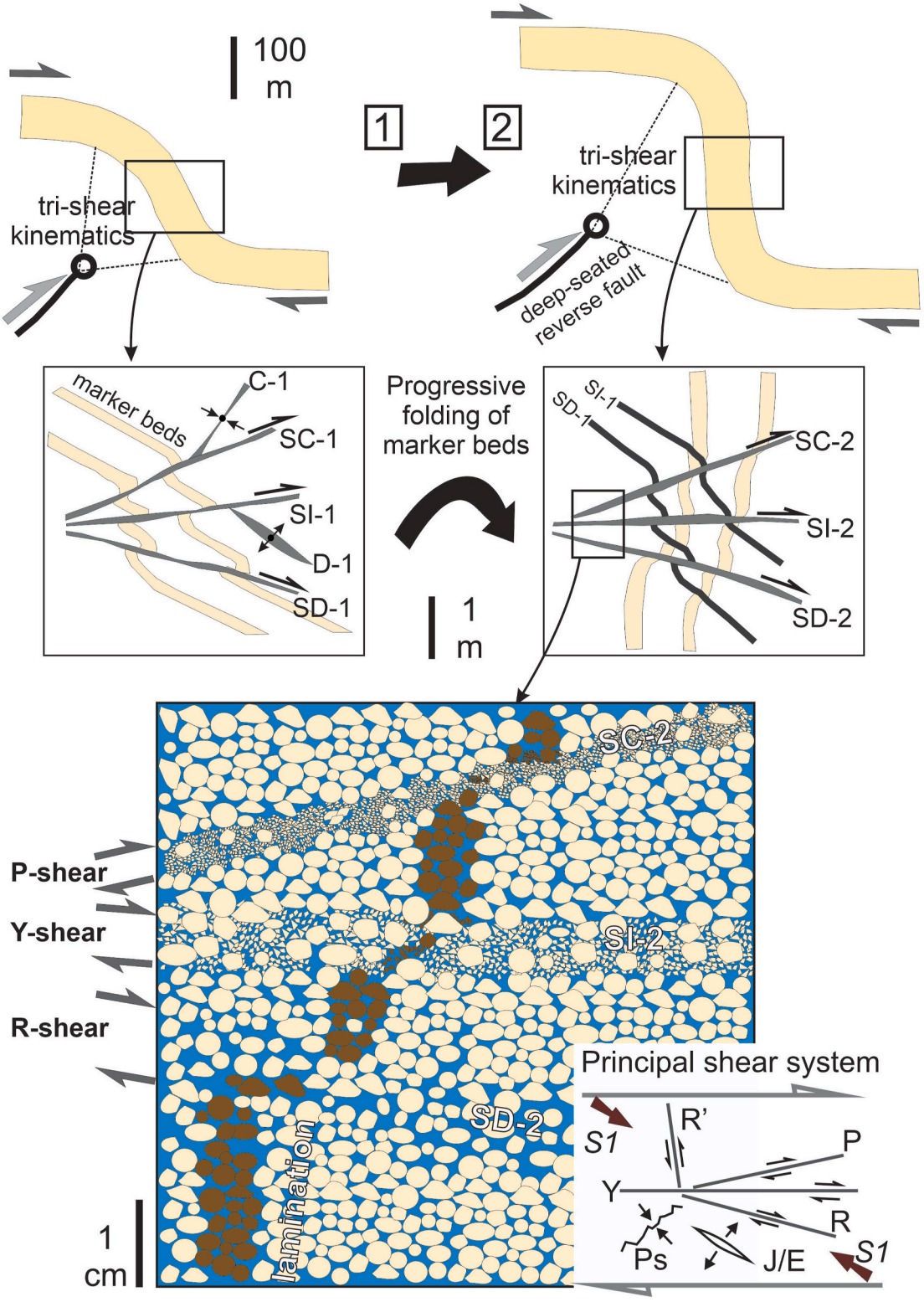

Fig. 1. Progressive folding of a sandstone succession (yellow layer), seen at stages 1 and 2 during continuous deformation on 100-m scale, depicted in a tri-shear kinematic fold model. On meter-scale, deformation is recorded as mainly discrete shear zones, or faults, that accommodate strain during folding. In highly porous sandstone discrete strain is mainly seen as deformation bands. The cm-scale drawing depicts yellow quartz (-feldspar) sand grains that hosts a lamina bearing heavy minerals (brown), representing a marker for shear offset. In detail, bands can be distinguished as shear-compaction (SC), shear-isochoric (SI) and shear-dilation (SD) structures, as well as compaction (C) and dilation (D) bands, depending on their orientation. Inset in lower right shows Riedel-classification for fractures; Y, P, R and R′ shear fractures, J/E for joints or extension fractures, and Ps for pressure solution seams, based in a principal shear system ascribed to a stress field ($\sigma 1 = S1$). Rather than stress, this contribution consider strain by shortening and extension axes. Similar conceptual classification can be ascribed to deformation bands for a principal shear system. In this study, the orientation of bands offers a bearing on deformation mechanisms, spanning from cataclasis to granular flow. Volumetric kinematics of bands covers extensional movement causing porosity increase (dilation), truly band parallel shear with no volume change (isochoric) and contraction by porosity decrease (compaction). (For interpretation of the references to colour in this figure legend, the reader is referred to the Web version of this article.)

documented by small-scale structures with different deformation mechanisms and kinematics.

The study site is in the Uneva Mine Canyon on the east side of the San Rafael Swell (Utah, USA), a regional monocline (Fig. 2). This km-amplitude N–S striking and east-facing monocline is one of many Laramide Orogeny structures that sit above deep-seated, basement-rooted reverse faults of the Colorado Plateau, recording crustal-scale deformation from Late Cretaceous until Eocene (e.g., Bird 1998; Yonkee and Weil 2015). Growth of the San Rafael Swell monocline has been linked to formation of mainly cataclastic deformation bands in Jurassic sandstones, as investigated by Zuluaga et al. (2014). With bands forming during contractional folding, the overall kinematics suggests a contrast to bands developed in extensional regimes where strain concentrates around faults. Studies of extensional faults show that deformation bands develop as precursors to faults or by progressive strain in tabular damage zones as faults accumulate increased displacement (Aydin 1978; Aydin and Johnson 1982; Shipton and Cowie 2001; Berg and Skar 2005; Torabi and Fossen 2009; Tueckmantel et al., 2010; Schueller et al., 2013; Braathen et al., 2013). Contraction-induced deformation bands appear to be more broadly distributed away from faults (Solum et al., 2010; Brandenburg et al., 2012; Ballas et al., 2012a; Soliva et al., 2013). Zuluaga et al.'s (2014) investigation of the San Rafael Swell monocline shows that band intensity, orientation and band-swarm characteristics vary along the frontal limb of the monocline, reflecting a gradient in strain intensity by folding from the centre of the major structure towards the fold-hinge terminations in the northern and southern fold tips. Further, deformation bands can be divided into superimposed populations of structures, reflecting evolving strain during progressive folding.

The uniqueness of our study lies in deeper investigation of distinct structural populations of progressive deformation stages and especially transitions in deformation style between deformation bands and fractures. This is revealed in the central part of the forelimb of the San Rafael Swell monocline, where the strain is at its highest. We show that a total of four populations of structures record different kinematics and deformation mechanisms, depending on orientation to sedimentary bedding within the first-order fold. Small-scale structures span from cataclastic shear-compaction and shear-isochoric bands to dominantly disaggregation shear-dilation deformation bands (e.g., Aydin et al., 2006; Fossen et al., 2007). Further, extension (joints) - and mainly shear fractures record transitions from band to fracture formation. All populations host several elements (bands, fractures) of this structural diversity.

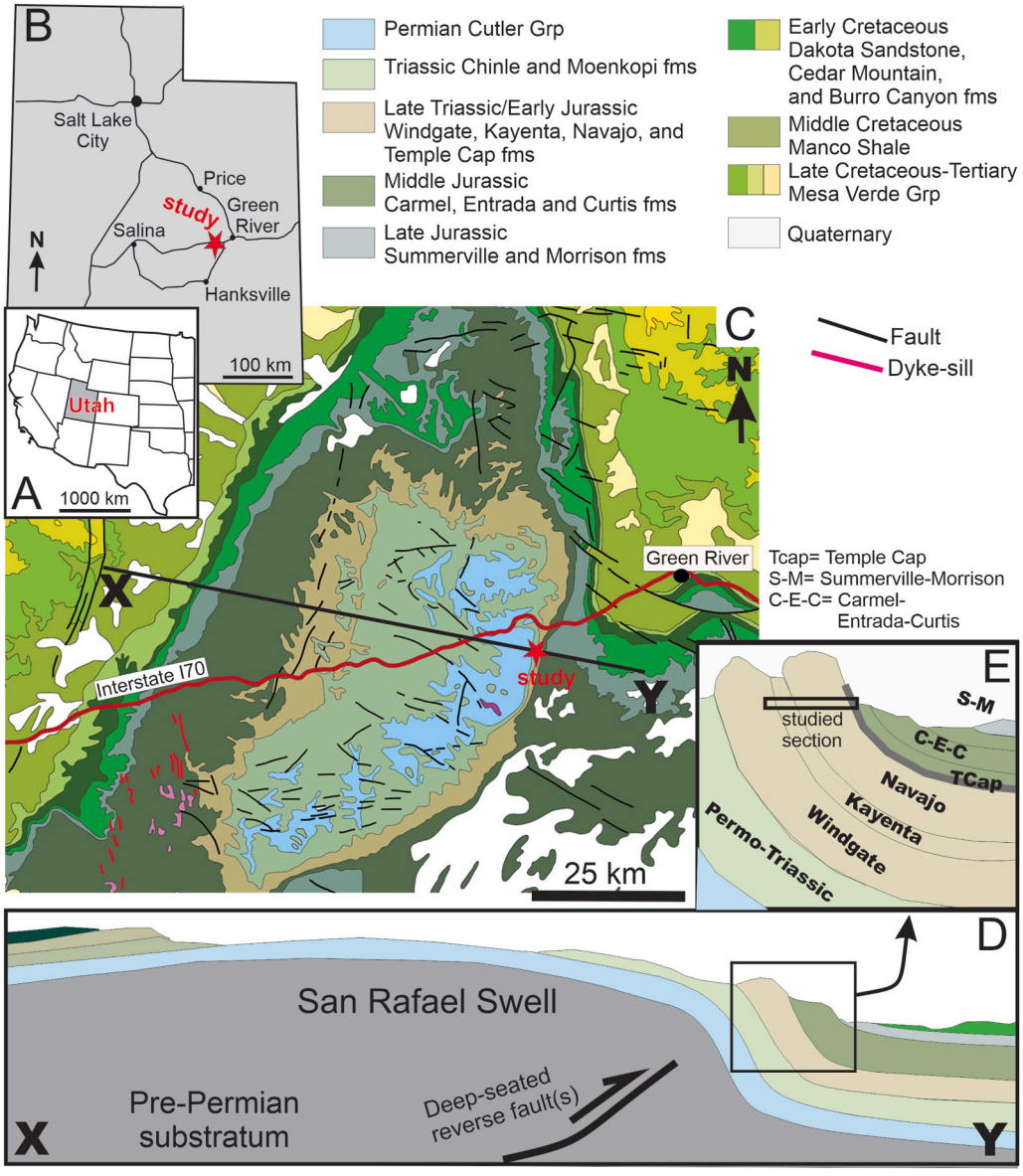

Fig. 2. (A) Utah State in the USA. (B) Location of study area in Central-East Utah. (C) Bedrock map covering central parts of the San Rafael Swell (modified from Hintze, 1980), locating the Uneva Mines Canyon and cross-section. (D) Cross-section X-Y showing the overall geometry of the San Rafael Swell monocline above a deep-seated reverse fault system rooted in metamorphic basement, (E) enlargement of the frontal, steeply east-facing limb of the monocline as shown in cross-section X-Y. The position of the Uneva Mines Canyon within the monocline is indicated. Cross-sections have horizontal equal to vertical scale.

2. Concepts, definitions and methods

Failure of rock by fractures causes dilation. Such structures can be divided into shear-fractures and joints, of which the latter records pure dilation, as for instance discussed in Aydin et al. (2006) and Schultz and Fossen (2008), and commonly applied to analysis of deformation in folds (e.g., Hancock 1985). Fractures can also be classified kinematically as Riedel shear structures (Riedel 1929) based on orientation within a localized shear-system (Petit 1987; Dresen 1991; Misra et al., 2009). The Riedel scheme is organized using common terms P-, R- and R′-shear fractures oriented within sectored angles around the principal shear direction/structure termed Y. T-structures recording pure dilation (= joint). Some controversy exists around the Riedel scheme, connected to changing rheological conditions and boundary stresses that are influenced/changed during progressive deformation, challenging the first-order connection between structural orientations and stress axes. Our approach is that of strain in a shear system - we advocate for stepwise occurrence of failure along preferred orientations along the lines of Schultz and Balsko (2003) and Aydin et al. (2006). For simplicity we apply the Riedel scheme on populations hosting seemingly concurrently formed structures of mainly R, P and Y shear deformation bands.

Shear-system classification has been applied to deformation bands around faults in porous sandstone (e.g., Ahlgren 2001; Schultz and Balsko, 2003; Braathen et al., 2009; Pizzati et al., 2020). The concept is based on a relationship between kinematics and orientation of deformation bands within a shear system, with similarities to the shear fracture classification introduced above, as explored by Schultz and Balsko (2003). The main difference is the response in the rock mass, which allow either contractional or extensional strain due to porosity adjustments besides shear along the band, as outlined in Fig. 1. We follow the consensus for classification of deformation bands, as summarized in Fossen et al. (2007) and in later literature (e.g., Aydin and Ahmadov 2009; Fossen 2010; Ballas et al., 2013; Skurtveit et al., 2013; Fossen et al., 2015). Deformation mechanisms are reflected in the spectra from grain-breaking cataclastic deformation bands to disaggregation deformation bands formed by granular flow. Bands volumetric kinematics are defined by movement across the band, from pure compaction or dilation by band-normal decrease or increase of porosity, respectively, to elements of shear incorporated in the band, as investigated for instance by Fossen et al. (2015) and Braathen et al. (2018). These observations are reflected in terms used herein, e.g., compaction -, shear-compaction -, shear-isochoric -, shear-dilation - and dilation deformation bands. Further, orientation of bands within a strain field influences loading on grain contacts. In highly porous sandstones, this could ultimately control different deformation mechanisms, from extensive cataclastic flow common in shear-compaction bands, to milder cataclasis in isochoric bands, and to mainly granular flow in shear-dilation bands, as illustrated in Fig. 1. In this paper we discuss progressive strain for 4 distinct Populations of deformation bands. We present the kinematic interpretations of deformation bands and fractures linked to their deformation mechanisms, spanning across to shear system discussions. Analysis of progressive strain in a major monocline sanctions discussions of tri-shear kinematics in folding.

The work presented here is based on systematic observation and measurements of deformation bands and fractures, collected in scanlines and at sites across the intensely deformed monocline hinge-zone. This analysis is paired with thin section analysis, and complemented by photographs and drone images. The latter were captured from around 300–400 m height above and partly inside the Uneva Mine Canyon. This composite image (Figs. 3 and 4) offers an overview of the 200–300 m deep and narrow (10–50 m wide) canyon, which is poorly covered in other remote sensing data. The image was used for locating the scanline and for logging and sampling.

The lithostratigraphic log shown in Fig. 4 provides a compilation of recorded sedimentary facies (grain size and sorting) and sedimentary architecture (10's of m) from beds (m's) to lamina (cm's – mm's), summarizing observations from both canyon walls. A structural geology scanline follows the stratigraphic strip-log (Fig. 4C); it was used to record dip of bedding, and the number and type of deformation bands (and fractures) per meter. Systematic description and analysis of small-scale deformation structures was done according to orientation, deformation style and cross-cutting relationships. These Populations were identified based in study stations (10 to >100 m^2 size), most located to canyon walls but a few on the canyon floor, as part of systematic description of small-scale deformation. These sites also host many cases of the aforementioned overprinting/cross-cutting structural relationships reflecting a systematic progression of deformation, and were used to establish a relative chronology for the Populations, from 1 to 4. Samples were collected from specific deformation bands and fractures using the interpreted framework of structural Populations. Further, patterns of mineral precipitates indicative of reactive fluid expulsion events were recorded as part of a parallel study (Sundal et al., 2016, and further work in preparation). Observations of diagenetic reactions contextualized in a framework of associated pressures and temperatures as well as the structurally induced opening of conduits, enrich the discussion of the deformation history. Nearly all structures and mineral phases were sampled in situ by drilling of plugs (2.5 cm diameter, 4–6 cm long).

Samples, predominantly from the Navajo Sandstone, were prepared into 15 thin-sections. Optical petrographic analysis of these thin-sections was done using a Nikon Eclipse Ci-POL microscope with a mounted high-resolution camera. Some thin sections were analysed in a Scanning Electron Microscope (Hitachi SU5000 at the Dept. of Geosciences, UiO), to extract high-resolution information on mineralogy and diagenetic sequences, including pore- and fracture-filling cements.

3. Regional setting

The north-south trending and east-verging San Rafael Swell monocline is one of many Laramide Orogeny fault-propagation folds of the Colorado Plateau, which developed above deep-seated reverse faults (Yonkee and Weil 2015). It has a length of around 70–80 km and a width of a few km's (Fig. 2). The monoclinal limb changes geometry along strike, from subvertical bedding in central areas, to gentle and subhorizontal dips near its northern and southern fold-tips, as outlined in Zuluaga et al. (2014). The study site of Uneva Mine Canyon is located south of the I-70 freeway and crosses the east-facing monocline limb near the most intense folding where beds dip 70-80° to the east and form cliffs. At Uneva Mine Canyon, the fold limb is incised, allowing access to fully exposed rock faces/cliffs through the stratigraphy.

The stratigraphic interval includes Palaeozoic to Mesozoic deposits (e.g., Hintze and Kowallis 2009), with the ridge line/reef forming cliffs formed by eolian deposits of the Late Triassic Wingate Sandstone and the Jurassic Navajo Sandstone, separated by a short section comprising intertonguing eolian and fluvial sandstones of the Kayenta Formation (Fig. 2). Overlying the Navajo Sandstone are the Jurassic Temple Cap, Carmel, Entrada, Curtis and Summerville formations (Hintze, 1980; Witkind, 1988; Doelling, 2001; Doelling et al., 2015; Zuchuat et al., 2018). Our study, investigates structural features within the Kayenta and Navajo to Temple Cap succession, with emphasis on deformation in the eolian deposits of the Navajo Sandstone.

Deformation in the Navajo Sandstone is extensively described in the literature, as it forms distinct cliffs that allow easy access to fault-related, mainly cataclastic deformation bands (e.g., Shipton et al., 2002; Skurtveit et al., 2015; Zuluaga et al., 2014). The Navajo Sandstone is classified as a fine-grained quartzite (>90% quartz grains), with porosity commonly in the range of 25–30% and permeability on the Darcy level (e.g., Ballas et al., 2015; Skurtveit et al., 2015; Zuluaga et al., 2014). Similar characteristics are suggested from our thin-section analyses, with image-based analysis of porosity offering values of 15–25% in the Navajo Sandstone, with the lower porosity reflecting infill by quartz, calcite and/or oxide cements (Sundal et al., 2016).

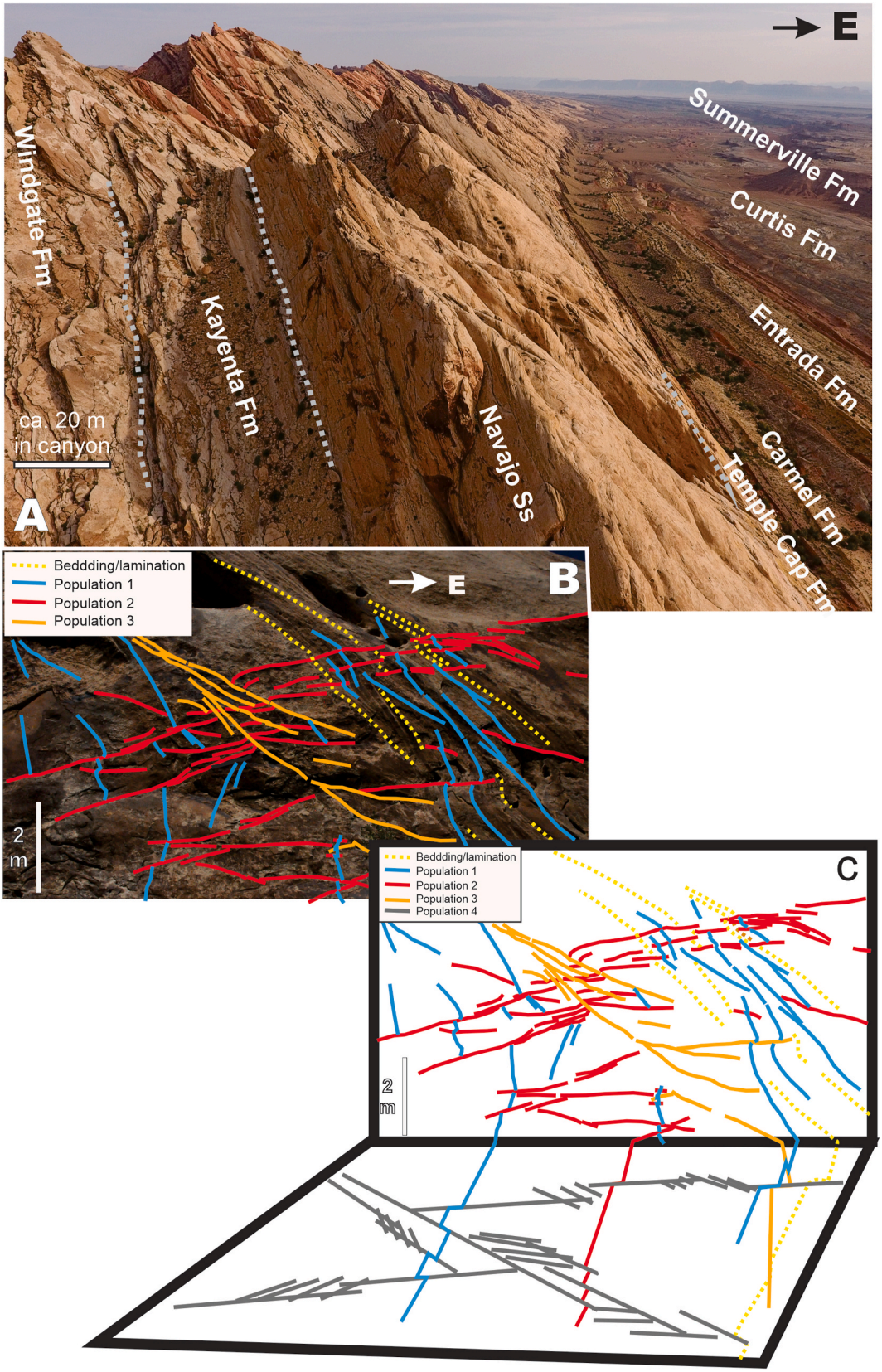

Fig. 3. (A) Drone image presenting an overview of stratigraphic units mentioned in the text. (B) Photograph of canyon wall near the entrance to the canyon, located in Fig. 4, showing Populations of chiefly deformation bands impacting bedding/lamination in the Navajo Sandstone. Distinct deformation band swarms of three Populations can be distinguished in the rock phase. (C) Schematic figure combining the rock-face shown in "B" with observations in the canyon floor. Folding of band swarms and truncating relationships document a chronology of deformation events, from the older Population 1 to the younger Population 4. Population 4 structures are only recorded in the canyon floor.

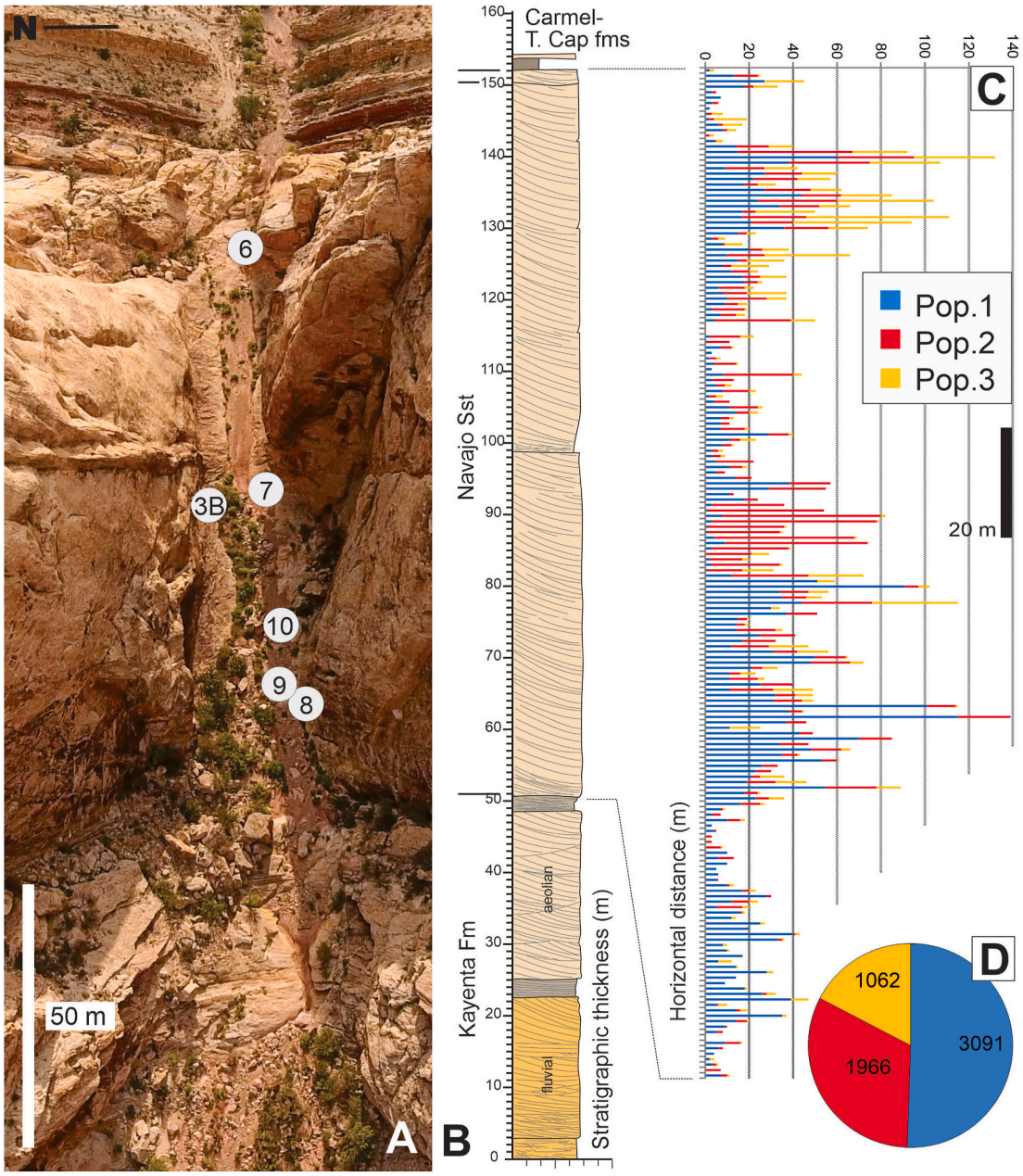

Fig. 4. (A) Drone photograph down into Uneva Mines Canyon, showing the narrow canyon in which the lithostratigraphic log and scanline are recorded. Specific sites of other figures are shown as numbers. (B) Lithostratigraphy recorded in the canyon, see text for description. (C) Scanline recording number of deformation bands per meter along the same line as the lithological log. Populations 1–3 are distinguished, whereas Population 4 with sub-vertical structures has been omitted because they are significantly under-represented in the scanline. (D) Pie-chart showing sectored concentrations and the number of Population 1–3 structures of the scan line.

Sandstone porosity and permeability reflects mild compaction and diagenetic modifications, with slight growth of grain-contact quartz as well as pore- and fracture-filling carbonate and oxide cements (Skurtveit et al., 2015; Sundal et al., 2016). Burial depth for the Navajo Sandstone during onset of the San Rafael Swell monocline folding is estimated to be in the range of 2.0–2.8 km (Zuluaga et al., 2014; Petrie et al., 2017), perhaps as deep as 4 km's (Sundal et al., 2016). There are no accounts for depth at the end of the monocline formation, but the km-amplitude folding will have created significant variations in burial of the involved formations.

4. Lithostratigraphy and sedimentary facies

In Fig. 4B, a lithostratigraphic log outlines the overall grain size and facies distribution of the studied succession. The Kayenta Formation displays a complex intertonguing architecture of sandstone-dominated, fluvial and eolian intervals (Averitt et al., 1955; Harshbarger et al., 1957), with spatio-temporal variability related to humid-arid climatic variations (Hassan et al., 2018; Priddy and Clarke, 2020). Fluvial channels are characterised by fine to medium-grained sandstone, sourced from adjacent eolian deposits, resulting in near-uniform grain-size distribution (excluding the very coarse-grained to granule-size conglomerates at the base of some of these ephemeral fluvial units), while overbank/floodplain elements mostly consist of rippled to laminated siltstone (Priddy and Clarke, 2020). Ultimately and as the aridity kept increasing, the Kayenta Formation was conformably overlain by the expanding Navajo erg, which explain the increasing concentration of eolian pulses towards the top of the formation

(Middleton and Blakey 1983; Hassan et al., 2018; Priddy and Clarke, 2020), as observed in Uneva Mine Canyon (Fig. 4) Intermittent beds less than 50 cm thick comprise very fine sand to silty ripple-laminated strata near the base of the studied section.

The Navajo Sandstone developed as a widespread erg, where tall eolian sand-dunes were separated by moist inter-dune areas close to a fluctuating groundwater table (Bromley 1992). Wind-flow separation at the dune crests led to well-sorted steep cross-sets of fine-grained sand, while finer fractions accumulated between dunes. Dune migration subsequently resulted in a well-defined bipartite Navajo Sandstone composition; foreset sandstone beds commonly exceeding 10 m thickness consists of well-sorted, well-rounded sand. Thin (up to 1 m) beds are chiefly composed of very fine sand and silt. The compound dunes prograde on supersurfaces (sensu Kocurek, 1988), or prograde directly on inter-dune beds. Tabular, decimeter (dm)-thick mudstone and sandstone beds, strikingly dark red, with parallel lamination make up inter-dune composite bedsets. This eolian dune and interdune composition form the basis on which the Navajo Sandstone responded to strain during formation of the San Rafael Swell monocline. Noticeably, both units develop deformation bands.

The Middle Jurassic Temple Cap Formation, previously referred to as the Page Sandstone, unconformably overlies the Navajo Sandstone at a significant erosional hiatus (J1 unconformity) in the study area (Sprinkel et al., 2011; Doelling et al., 2013, 2015; Zuchuat et al., 2019a, 2019b). The Temple Cap Formation developed as an eolian erg, with several tens of m thicknesses in outcrops to the south of the San Rafael Swell (e.g. Havholm and Kocurek 1994). The Temple Cap Formation is, however, less than 3 m thick in the study area, and is composed of well-sorted eolian sandstone with tangential cross-stratification reflecting compound desert dune development (Sprinkel et al., 2011; Doelling et al., 2013, 2015).

5. Deformation structures

Distinct narrow, tabular zones of deformation bands (swarms) can be distinguished in the cliff faces of the canyon, as shown in Fig. 3B. Older structures are represented by Population 1 bands with west-directed shear, in many cases with structures merging with primary lamination and bedding. Population 2 structures reveal east-directed shear and are superimposed by the younger, Population 3 structures of west-directed shear. Population 4: subvertical structures, represents the youngest deformation event; cross-cutting all former Populations and is not observed on the scanline due to its orientation relative to the scan line sample.

There is an overall trend in deformation patterns, with early, widespread deformation throughout the succession of Population 1 structures, followed by more discrete zones of deformation represented by populations 2 and 3. The number of structures within the Populations shows a decreasing number from Population 1 to Population 3, with nearly half the recorded structures belonging to Population 1 (Fig. 4). Distribution-wise, Population 1 structures are present throughout the scanline, albeit with higher frequency in the lower succession, and at the interface between thicker eolian beds and thinner beds. Population 2 is most prominent near the top of the lower major composite dune (around 90 m) and Population 3 structures have a stronger expression towards the top of the succession, and also offer sections with distinct clusters. Population 2 structures show a greater clustering, mainly in or near inter-dune layers, where they are frequent. This contrasts to sections with minimal Population 2 impact. For Population 3, a similar clustering is present, but for this Population there are sections without presence of structures. Population 4 structures are sub-vertical, and found in the canyon floor, mainly at two locations (9 and 10 in Fig. 4A). Their scattered appearance suggests they are strongly clustered, and separated by barren intervals.

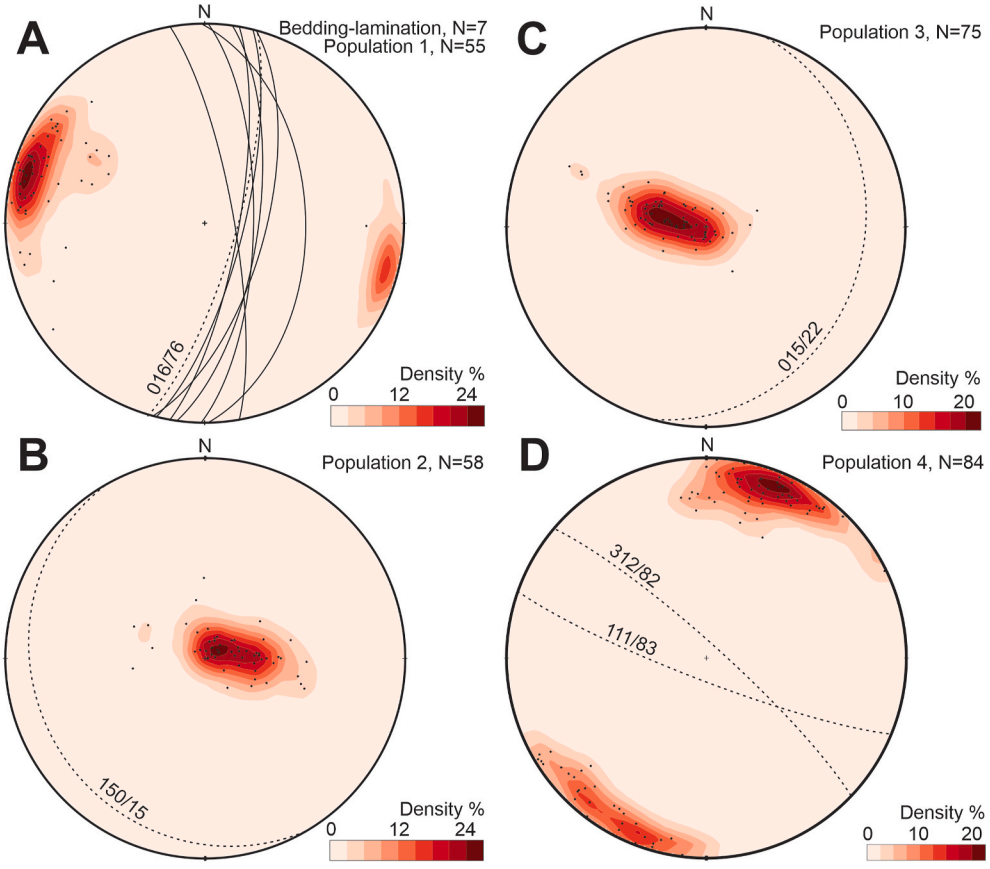

Fig. 5. Stereoplots showing orientation of recorded structures of Populations 1–4 (lower hemisphere, equal area stereonet). Dashed great circles represent average structural orientations. (A) Population 1 deformation bands plotted as pole to plane and contoured, and bedding/lamination planes as great circles. (B) Population 2 structures plotted as pole to plane and contoured. (C) Population 3 structures plotted as pole to plane and contoured. (D) Population 4 structures plotted as pole to plane, with two planes representing two average structural sets given by two pole-to-plane clusters.

Population 1 structures have an overall steep to sub-vertical ESE dip, subordinate sub-vertical to the WNW (Fig. 5). These structures are sub-parallel to parallel to the steeply east to ESE dipping bedding in the frontal limb of the San Rafael Swell monocline. Population 2 structures dip mainly gently westwards, whereas Population 3 structures predominantly display a gentle to moderate easterly dip. Population 4 structures are sub-vertical and divide in two sets; both striking NE-SW. A narrow, ~30°, bisector between the sets gives a symmetry (shortening) axis trending ca. 125-305°.

5.1. Population 1

Population 1 comprises cataclastic deformation bands that are sub-parallel to the steeply east-dipping bedding, in accordance with the account of Zuluaga et al. (2014). They appear as isolated bands or narrow centimetres (cm) to decimetre (dm) wide band swarms (Fig. 6).

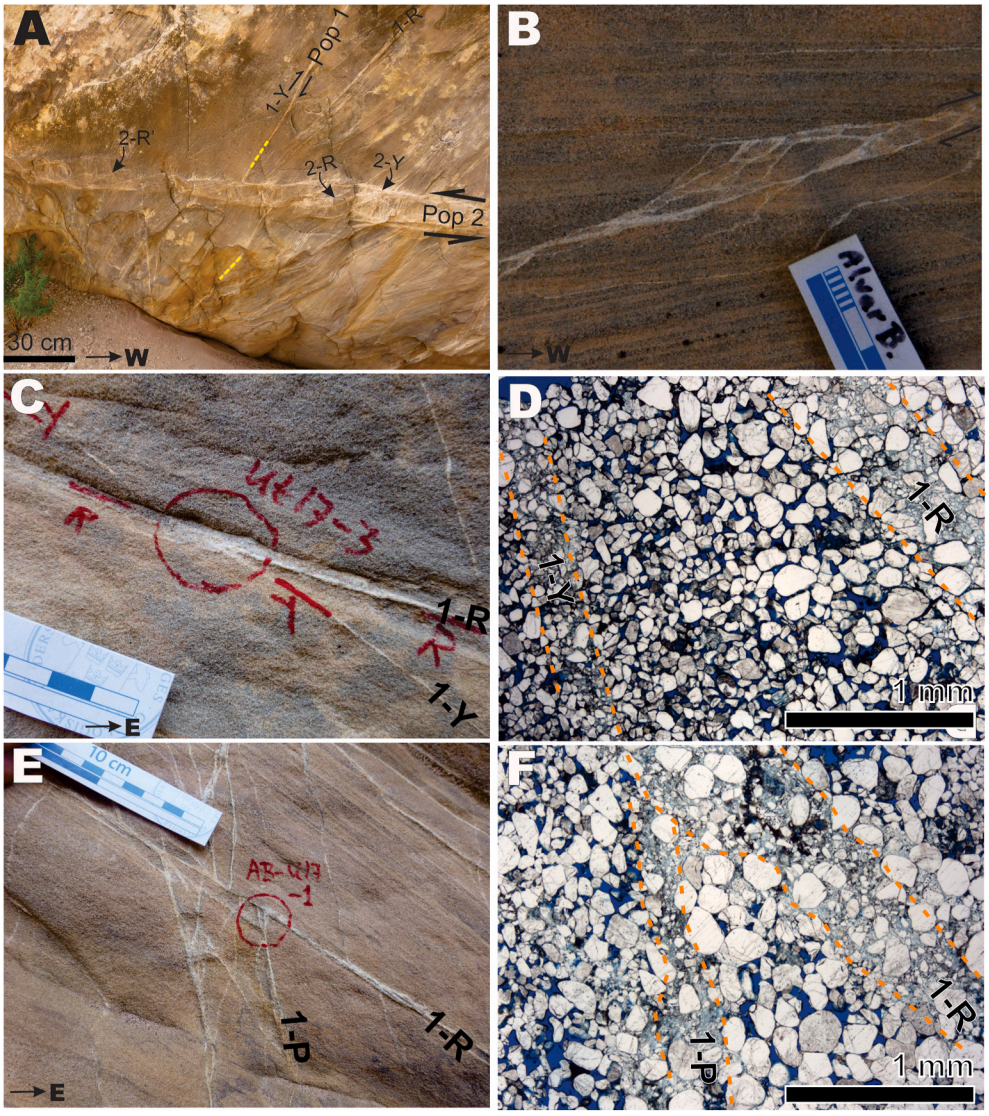

Fig. 6. (A) Photograph of Population 1 structures truncated by a Population 2 deformation band swarm made up of mainly R-bands and bounding Y-bands. Some R′-bands can be seen to the left/east. Note ca. 30 cm top-to-the-east (top-E) offset of the yellow marker representing a Population 1 band swarm. Bands are ascribed Riedel shear terms based in their orientation within the shear system, as outlined in Fig. 1, with number representing the respective Population (e.g., 1-Y= Y-shear of Population 1). (B) Photograph of Population 1 deformation bands in thick, highly porous dune sandstone (porosity > 25%). Bands are partly following primary lamination or cutting up-section towards the west. Along the bands, cm-scale top-W offset of lamination is visible. (C) Photograph of two sets of Population 1 deformation bands (Y and R), of which the Y-band slightly (mm-scale) displace the R-band in a top-W direction (inside red circle). Such truncations are however inconsistent for this site. (D) Photomicrograph of thin-section made from a plug drilled out normal to the rock-face at the encircled site in "C". Blue colour is epoxy resin that fills porosity. The R-band follows a thin bed/lamina with slightly larger grain size compared to the Y-band that cut lamination with a low angle. Grain size may be of relevance, in that the Y-band is narrower than the R-band, which is also visible in the thin-section. Both the Y and R-band show a fine matrix surrounding some larger grains, and minimal porosity. Accordingly, both bands record cataclasis and shear-compaction. (E) Photograph of Population 1 deformation bands classified as R and P structures. The vertical bands are P-structures that cut lamination, whereas the R-band appears as a swarm that overall follows dune lamination. Consistently for this site (but not in general), the R-bands cut and offset the P-band with ca. 2-cm in a top-W direction. (F) Photomicrograph of thin-section from drilled plug (circle in "E"), which shows an overall thicker R-band compared to the P-band. In detail, the P-band reveals a bimodal grain size distribution, with a few survivor grains in a clay-fraction matrix. The R-band has a polymodal grain-size distribution, with numerous intermediate size angular grains in addition to the very fine matrix and several survivor grains. Both bands classify as cataclastic shear bands, but the intensity of deformation as indicated by grain-size reduction appears higher in the P-band. (For interpretation of the references to colour in this figure legend, the reader is referred to the Web version of this article.)

Areas of band intersections locally create ladder-structures, most common in bed-interface areas. Population 1 structures either follow primary lamination or cut up/down-section towards the west at a low angle (<20°) to bedding (Fig. 6B). The width of deformation bands varies, with R-bands consistently showing a wider deformation zone (<5 mm) than Y and P bands, as seen in Fig. 6C and E. Where Y, P and R-structures can be identified together, the R structures appear to be the structural set that follows lamination. For all bands, top-to-the-west (top-W) offset of lamination or pre-existing bands are commonly visible (e.g., Fig. 6B), showing up to 1 cm of displacement. Band truncations within Population 1 are common; however, there is no consistent chronology of offset, suggesting the bands formed in unison within a consistent strain field.

Most of Population 1 structures classify as cataclastic shear-compaction bands, showing a very fine-grained matrix surrounding larger survivor grains, and significant reduction in porosity compared to the host-rock. There is, however, higher porosity within R-bands (c. 10%) compared to the other band sets, suggesting these bands experienced less compaction. These R-bands denote transitions towards shear-

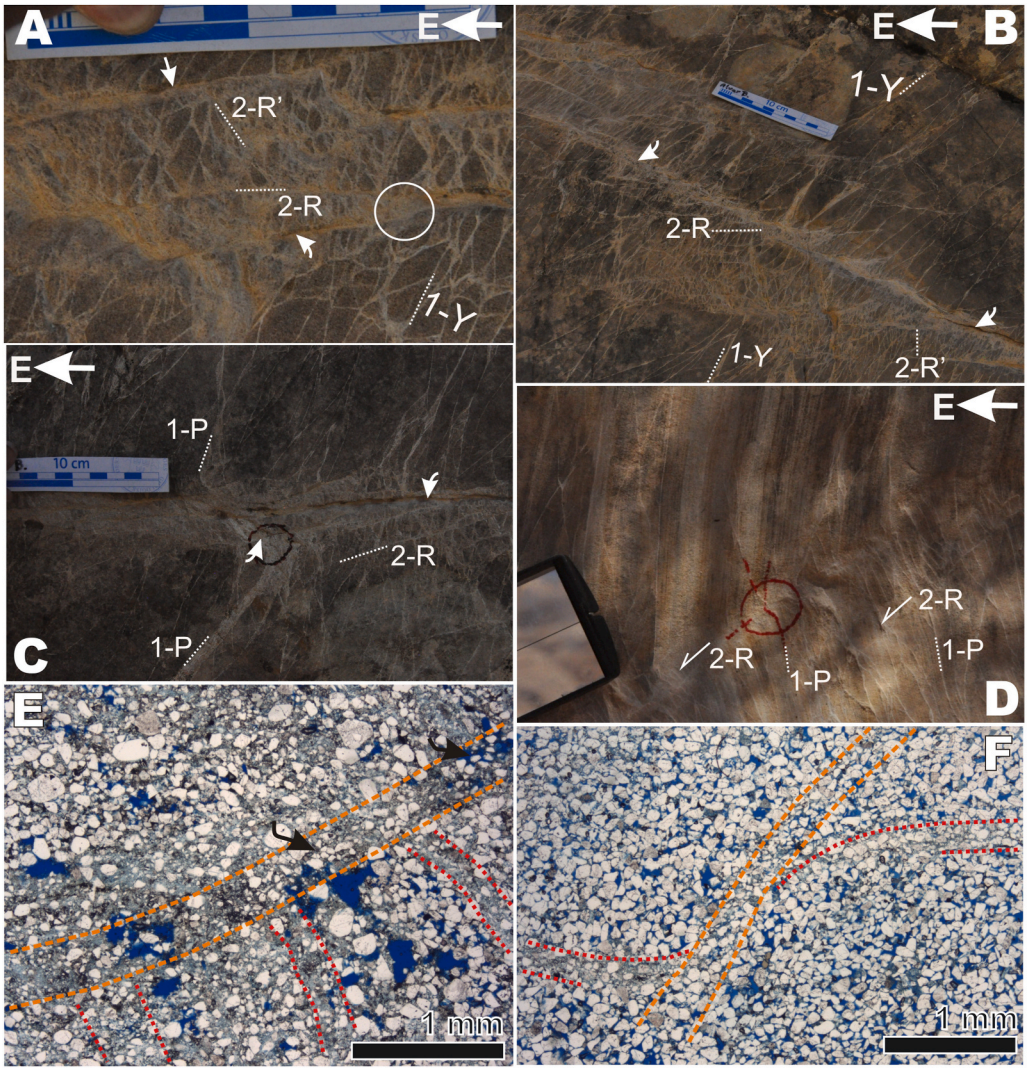

Fig. 7. (A) Population 2 deformation band swarm consisting of R and numerous interconnecting R′ structures. Along the R-bands there are dm-long patches of shear fractures, located with arrows. Both the bands and shear fractures show top-E offset. Fractures can be seen to tip out in deformation bands (circle). Population 2 bands are superimposed on Population 1 bands (annotated 1). (B) Population 2 deformation band swarm consisting of Y, R and R′ bands. R-bands curve into the Y-orientation, creating a composite Y-band swarm. Patches of shear fractures (arrows) are found along the Y-band swarm. (C) Population 2 deformation band swarm consisting of Y and numerous R structures, the latter connected by numerous, cm-long R′-bands. Shear fracture patches (arrows) appear both along Y and R bands. A narrow band swarm of Population 1 can be traced through the Population 2 swarm in the shape of an east-verging fold. In the fold, offset of the Population 1 band swarm by R and Y structures of Population 2 are on cm-scale. (D) Dm-spaced set of R-bands of Population 2 folds and/or truncate Population 1 bands. (E) Photomicrograph of thin-section from plug drilled out of black circle in "C". The rock shows extensive grain size reduction (cataclasis) throughout; some Population1 bands, or rather high-strain zones (outlined in red) within band swarms stops at the margin of a Population 2 band(s) (orange), suggesting Population 2 bands truncate Population 1 bands in accordance with the offset recorded in the outcrop. A fracture tips out in the upper right corner (arrow) and a possible < 2-cm long hairline fracture is located by an arrow in the centre. (F) Photomicrograph of thin-section from plug drilled out of the red circle in "D". Here, the Population 1 band (red) is folded and offset by a Population 2 band (orange). Note that the R-band of Population 2 shows mild grain size reduction and has maintained significant porosity, with porosity nearly as the surrounding sandstone. Further, the Population 2 band is wider than the Population 1 band; the latter shows significant grain size reduction and offers minimal porosity. (For interpretation of the references to colour in this figure legend, the reader is referred to the Web version of this article.)

isochoric bands.

Both bimodal and polymodal grain-size distributions are present within the bands. For the Y and P bands there are a few survivor grains in a very fine-grained matrix (Fig. 6D); the R-bands show numerous intermediate size angular grains in addition to many survivor grains in the fine-grained matrix (Fig. 6D vs 6 F). Arrangements of grain size fractions within the bands suggest variable intensity of deformation, with most substantial grain destruction in the narrower P-bands. However, deformation band compositions ascribed to grain breakage and splaying (comminution) could also be influenced by subtle, lamina-scale grain size variations in the host rock, or by variable cataclasis controlled by shear offset accommodated by the band (Pizzati et al., in press).

5.2. Population 2

Population 2 comprises cataclastic deformation bands in localized zones, of which some band swarms host shear fractures, similar to the report of Zuluaga et al. (2014). They dip overall gently west, subordinately gently east, and cut bedding at a high to moderate angle. Both individual bands and band swarms show top-E offset of bedding/-lamination and earlier developed Population 1 bands, ranging 1–50 cm displacement.

From broader zones of dispersed bands, individual bands merge into band swarms, as shown in Fig. 7A–C. Typically, these sites show longer R-bands interconnected by numerous R′-structures forming ladder structures. Where distinct Y-structures are developed, they are located within en-echelon series of R-bands, of which some curve into the Y-orientation, creating a composite Y-band swarm. In band swarms with a substantial number of bands and larger offset of primary lamination, fractures are developed. In outcrop they appear as dm-long patches along both R and Y bands, with Y-bands offering longer and more linked fractures (Fig. 7C). Additional cm-long hairline fractures are visible in thin-sections (Fig. 7E). Both R and Y-parallel fracture sets show offset of markers similar to the hosting deformation band (swarm); hence, they are shear fractures. Further, the fractures tip out within the deformation bands, suggesting a physical interrelationship between band and fracture formation. These fracture networks probably correspond to the slip-surfaces reported by Zuluaga et al. (2014).

There is no obvious variation in the width of Population 2 bands compared to their orientation. All Population 2 bands classify as cataclastic shear-compaction bands, showing a very fine-grained matrix surrounding larger survivor grains, and significant reduction in porosity compared to the host-rock. However, in a few places R-bands show mild grain size reduction and has maintained significant porosity (Fig. 7F), in contrast to the significant grain size reduction encountered in the narrower Population 1 bands. R-bands of Population 2 classify as shear-isochoric bands.

5.3. Population 3

Population 3 consists of cataclastic deformation bands in localized zones, seen either as individual bands, or narrow, tabular band swarms (Fig. 8). They dip overall gently east, subordinate gently west, and cut bedding at a high angle. Individual bands and wider band swarms of Population 3 show top-W offset of bedding/lamination and earlier developed Populations 1 and 2 bands, on the cm to dm scale, respectively. Relay zones between bands and/or band swarms occur as localized ladder structures. Compared to Populations 1 and 2 structures, Population 3 bands are more sporadic with most structures present near the top of the Navajo sandstone.

Similar to Population 2 bands, there is no obvious variation in the width of bands related to their orientation. As with Population 2 bands, Population 3 classify as cataclastic shear-compaction bands. Population 3 bands have significant reduction in porosity compared to the host-rock; they consist of a very fine-grained matrix surrounding a few larger survivor grains. Fractures are found in a few Population 3 band swarms, which is similar to Population 2, but less common. They appear as cm to dm long patches along both R and Y bands. With fractures tipping out within the deformation bands, there is a physical interrelationship between band and fracture formation.

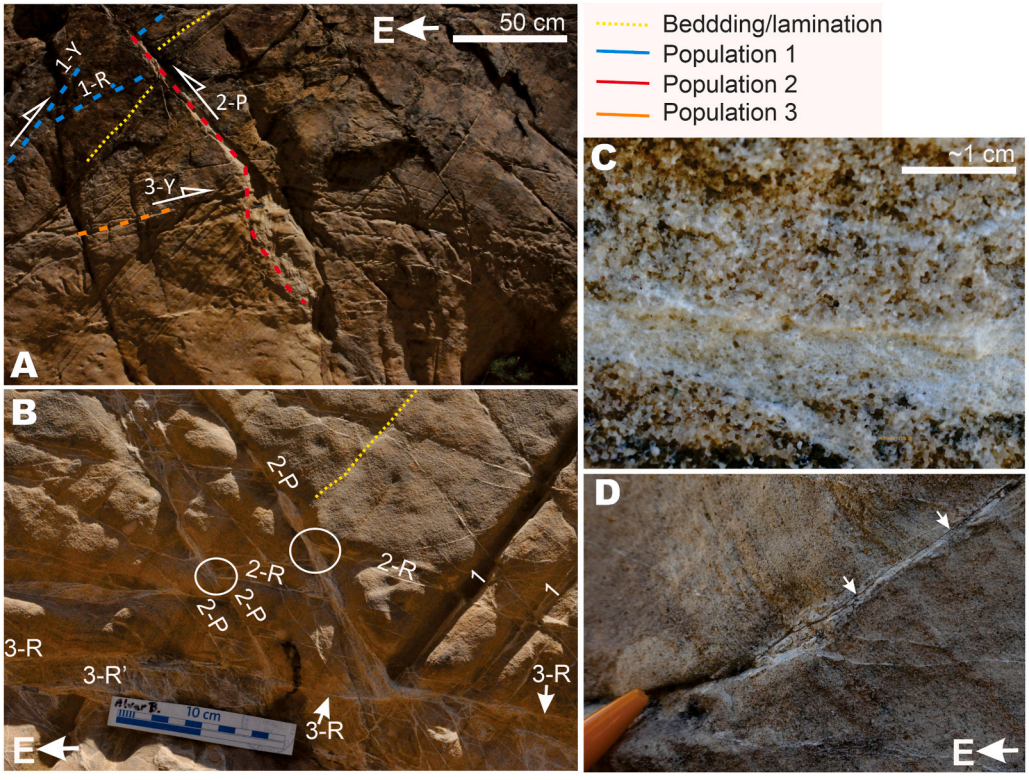

Fig. 8. (A) Photograph of Population 3 bands, superimposed on Populations 1–2 structures. There is top-E offset of sandstone lamination and Population 1 bands by a narrow Population 2 band swarm. The latter appears folded across a narrow band swarm of Population 3. (B) Close-up photograph of Populations 1-2-3 bands. In this case, P- and R-bands of Population 2 (2-P and 2-R) converge without visible mutual offset (encircled), suggesting they are formed in temporal harmony. In lower parts, the 2-P band swarms are offset by a narrow zone of R-bands of Population 3 (3-R) in a top-W direction. To the left, the 3-R band zone broadens into a ladder structure of short 3-R′ bands linking two narrow 3-R band swarms. (C) Close-up photograph of narrow 3-R band swarm, consisting of an up to 2 cm tabular zone in which individual bands are not clearly discernible; they are recognized by parallel laminae with grain size variations that at places branch out as individual bands. Survivor sand grains rest in a white, very fine-grained matrix. (D) Narrow Population 3 band swarm (3-P) that show connected fracture patches (by arrows). Pencil tip for scale; view to the south.

5.4. Population 4

Population 4 structures consist of two sets of mildly cataclastic deformation bands, disaggregation bands and shear fractures. These structures are partly cemented by calcite and/or Mn-oxides. Population 4 structures are superimposed on the other Populations. For the two sets, there is no consistent cross-cutting relationship, suggesting they are coeval. The two distinct sets are both sub-vertical, striking NW-SE. With the two sets showing different kinematics, i.e. dextral and sinistral offset, respectively, there is a narrow bisector for the shortening axis that is oriented 125-305° (Fig. 5C). This axis is slightly oblique to the regional trend of shortening represented by the San Rafael Swell monocline in this area.

As shown in Figs. 9 and 10, Population 4 structures are either individual shear structures or they appear as dm-wide zones, the latter showing en-echelon R-structures with a few connecting Y-structures. As all structures show mm to cm-scale offset of former deformation bands and primary lamination/bedding, there is evidently an element of shear displacement. No pure dilation structures were observed.

Individual shear structures are mainly disaggregation deformation bands that transgress into shear fractures (Fig. 10D) along strike. Hence, individual structures represent a combination of deformation bands and fractures. Notably, the bands show overall dilation with increased porosity, suggesting they are disaggregation shear-dilation deformation bands. Fractures in along-strike position display fracture walls follow grain contacts rather than cutting grains, except where Population 4 structures truncate Population 1 cataclastic deformation bands: here distinct fractures form (Fig. 10D). Albeit there is a shear component to the fractures, the width of the fractures suggests that they record a significant rate of dilation.

The dm-wide zones of composite R and Y-structures show structural elements that are similar to the individual structures described above; disaggregation shear-dilation bands transgress into fractures and back to bands. However, for some of the fracture walls there is grain-size

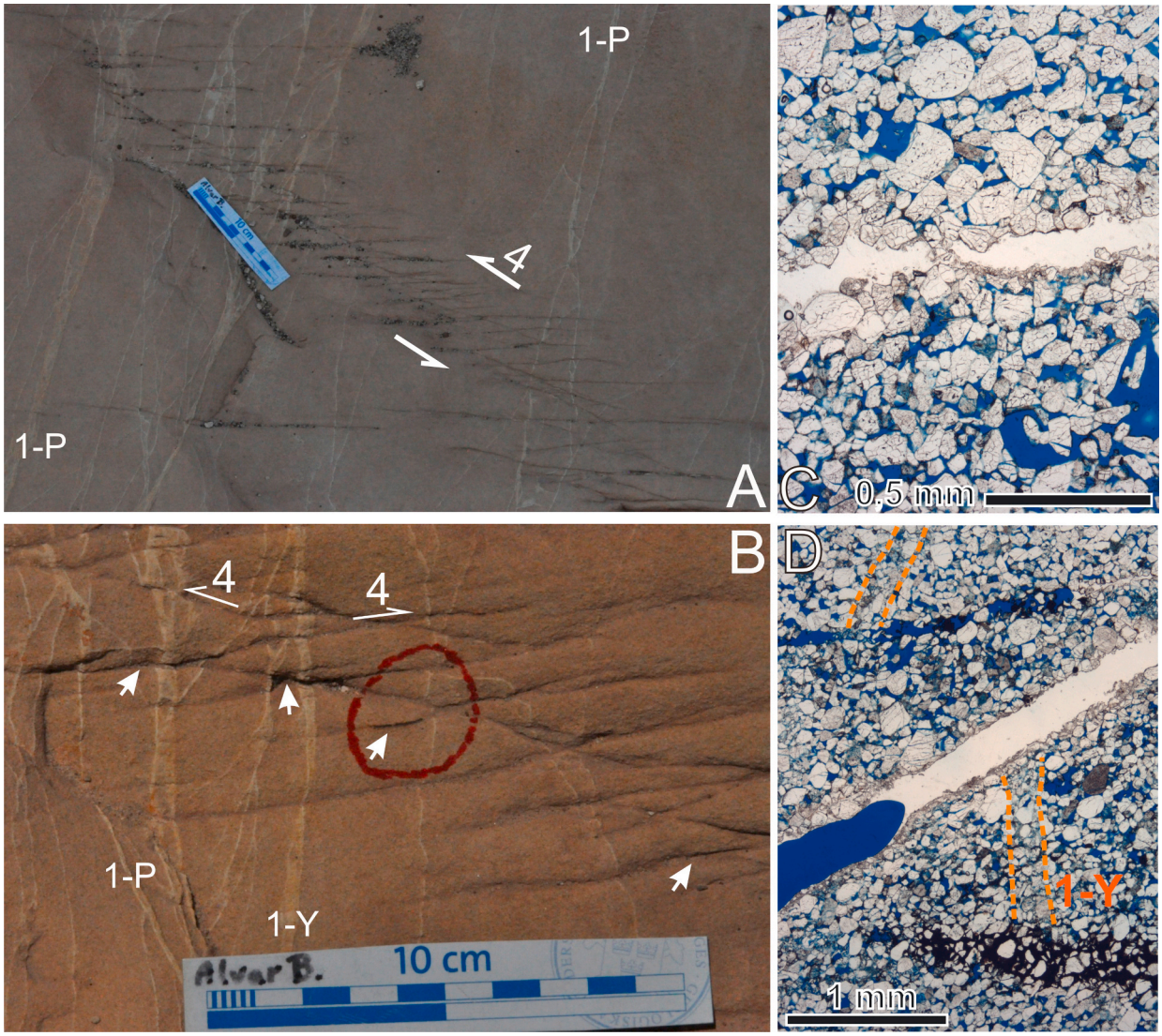

Fig. 9. (A) Photograph of Population 4 structures superimposed on Population 1 bands. The Population 4 structures appear as en-echelon R-shear bands, with a few connecting Y-shears, with both sets displacing Population 1 bands. (B) Detailed view of Populations 1 and 4 structures. Note shear offset of Population 1 bands by Population 4 structures. The Population 4 bands host dm-long shear-fractures, located by arrows. (C) Photomicrograph of Population 4 band with a calcite-filled fracture. Note denser grain packing and some grain breakage in the fracture walls. The fracture wall texture is consistent with that of a deformation band away from the fractured part (outside photomicrograph), indicating the fracture splits a pre-existing band. (D) Photomicrograph of thin-section made from plug drilled out of circle in 'B'. Population 1 cataclastic deformation bands are truncated by three Population 4 structures. At the base, there is a disaggregation shear-dilation band cemented by black oxides (MgO). Above, there is a partly calcite filled fracture with wall-rock grain size reduction and compaction. Further up, a shear fracture cuts a Population 1 band. In this case, there is no obvious deformation in the fracture walls.

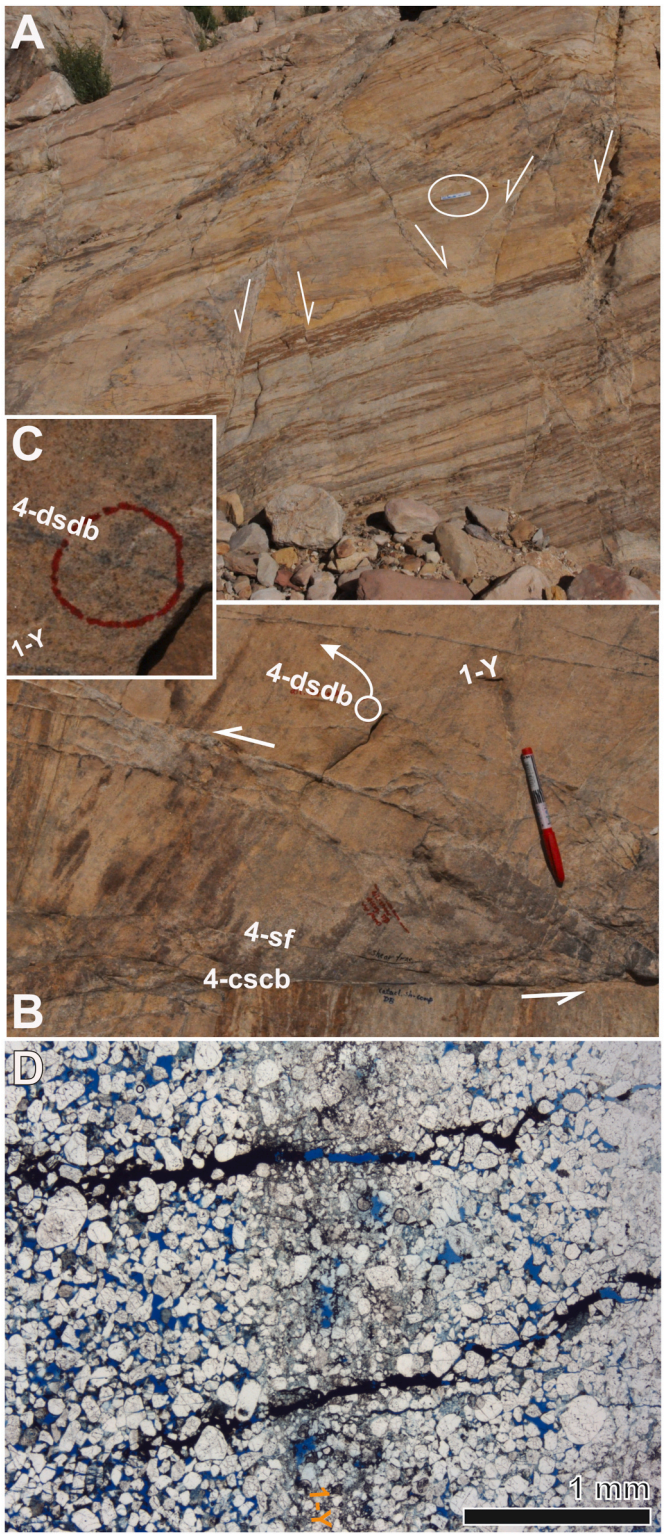

(caption on next column)

Fig. 10. (A) Conjugate sets of Population 4 structures, showing cm to 20-cm offset of primary lamination in the sandstone. The structures are composite disaggregation deformation bands and shear fractures. Note 10-cm long scale-bar (encircled). (B) Population 4 structures are made up of disaggregation shear-dilation bands (dsdb) hosting shear fracture (sf) patches, impregnated or filled with black and brown oxides (mainly MgO). Truncated Population 1-Y bands classify as cataclastic shear-compaction bands. (C) Photograph showing details of area in circle of "B", with mild sinistral shear folding of Populations 1 band across a Population 4 structure. The ca 2,5-cm wide circle locates the plug drilled out of the outcrop and made into a thin-section, shown in 'D'. (D) Photomicrograph of Population 1 band (top to bottom) cut by Population 4 fractures partly filled with black oxides (MgO). Note how fractures are following grain boundaries, and how the lower fracture is merging with a disaggregation shear-dilation band impregnated by oxides (lower left corner). Further, where Population 4 structures cut cataclastic Population 1 bands, a distinct fracture with semi-planar walls are present. . (For interpretation of the references to colour in this figure legend, the reader is referred to the Web version of this article.)

reduction. Along strike of these structures, there are patches of mildly cataclastic deformation bands giving way to disaggregation bands. Textural observations (thin sections) indicate that cataclasis is localized to small areas with pressure dissolution on grain contacts associated quartz overgrowths; however, this is not fully verified (Fig. 9C and D). These observed relationships suggest that the fractures split cataclastic deformation bands rather than that wall-rock grains collapsed during shear on the fractures (as common for slip-surface; e.g., Aydin and Johnson 1978; Tueckmantel et al., 2010).

6. Discussion

6.1. Deformation in monocline

Growth of folds such as the San Rafael Swell monocline is facilitated by gradual development and continuous deformation of layers, conforming to models describing a triangle zone of penetrative deformation in a fault-propagation fold (Erslev 1991; Cardozo et al., 2011) and in a tri-shear model, as explored for the San Rafael Swell monocline by Zuluaga et al. (2014). Folding-associated strain may offer elements of contraction or dilation when evaluated at a high (dm-m scale) resolution. For instance, Ismat and Mitra's (2005) advocated, in their investigation of fracture systems in larger folds of the Sevier fold-thrust belt in Utah, for collective movement on fracture-networks and faults at small scales in an elasto-brittle, cataclastic flow deformation mechanism, in sum contributing to the folding. Fractures record dilation, hence suggesting sub-simple shear strain during fold growth. For the San Rafael Swell monocline, folding triggered the formation of mainly shear-compaction deformation bands, conforming to contractional sub-simple shear strain unless counterbalanced by the subordinate fracture system (dilation).

Continuous deformation as recorded by the San Rafael Swell monocline was partly achieved by a cataclastic flow deformation mechanism, seen as small-scale discrete structures. These structures progress from overall bedding-parallel distributed, semi-penetrative shortening structures to discrete shear zones during monocline growth, ending with monocline-oblique contraction and extension (Fig. 11). In light of the distribution of structures in the various Populations encountered in the Navajo Sandstone, strain appears to be more evenly distributed and hence sub-penetrative at an earlier stage, as seen for Population 1 in Fig. 4C. Populations 2, 3 and 4 record progressively more pronounced localization into band (-fracture) swarms, which for Populations 2 and 3 appear more frequent near bedding interfaces and especially near the top of the unit. This suggests that the bedding orientation plays a role during early fold growth, as long as beds are orientated near-parallel to the shortening axis of folding, as also explored by Zuluaga et al. (2014). At this early stage the sandstone

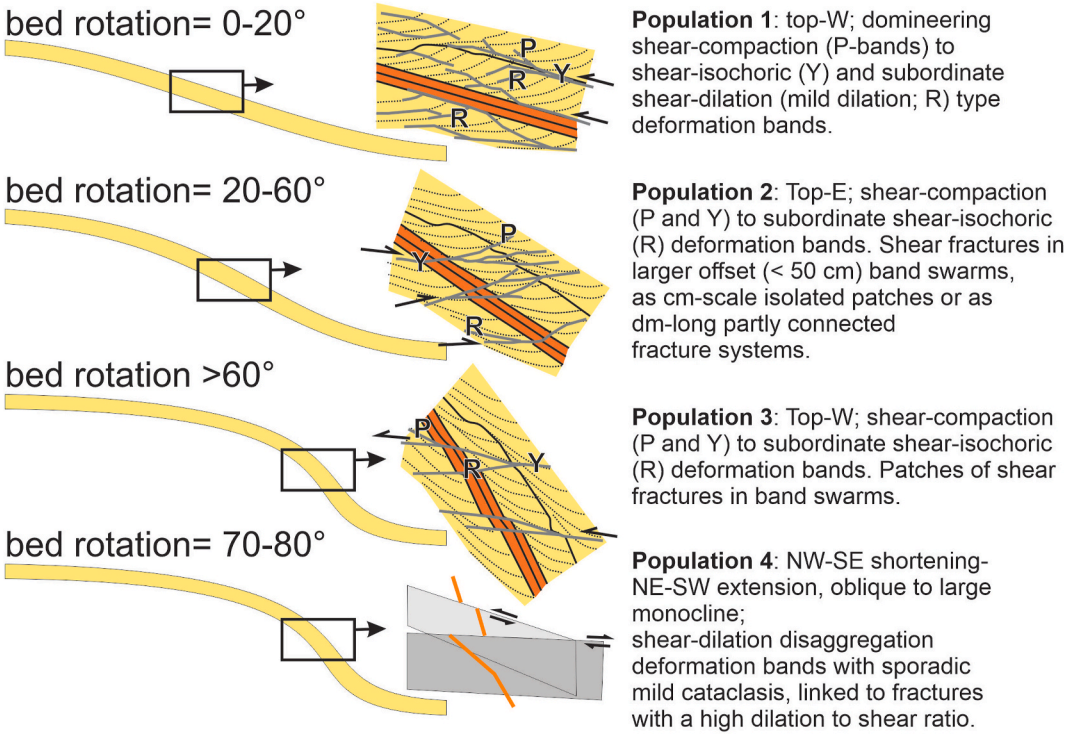

Fig. 11. Illustration of evolving strain field during folding, bridging from the chronology of structural Populations to growth of the San Rafael Swell monocline. Band orientations in sub-simple shear strain field influence deformation mechanisms within bands as they appear in the contractional sector (P), along the isochoric line (Y) or in the dilational sector (R). For details on strain interpretations, see Fig. 12.

experienced overall layer-parallel shortening and layer-normal thickening. During the early evolution, flexural-slip strain is considered unlikely due to penetrative strain and a lack of distinct bedding-interfaces within a fairly homogenous Navajo Sandstone. With progressively more inclined bedding, shear systems propagated across beds at higher angles and became dominant, likely with nucleation points representing the seed to progressive deformation in localized deformation zones. This may be envisioned in several ways, as demonstrated in Figs. 11 and 12: (1) In tri-shear models of folds, as for instance shown by Cardozo and Anonsen (2009), near-horizontal displacement vectors display

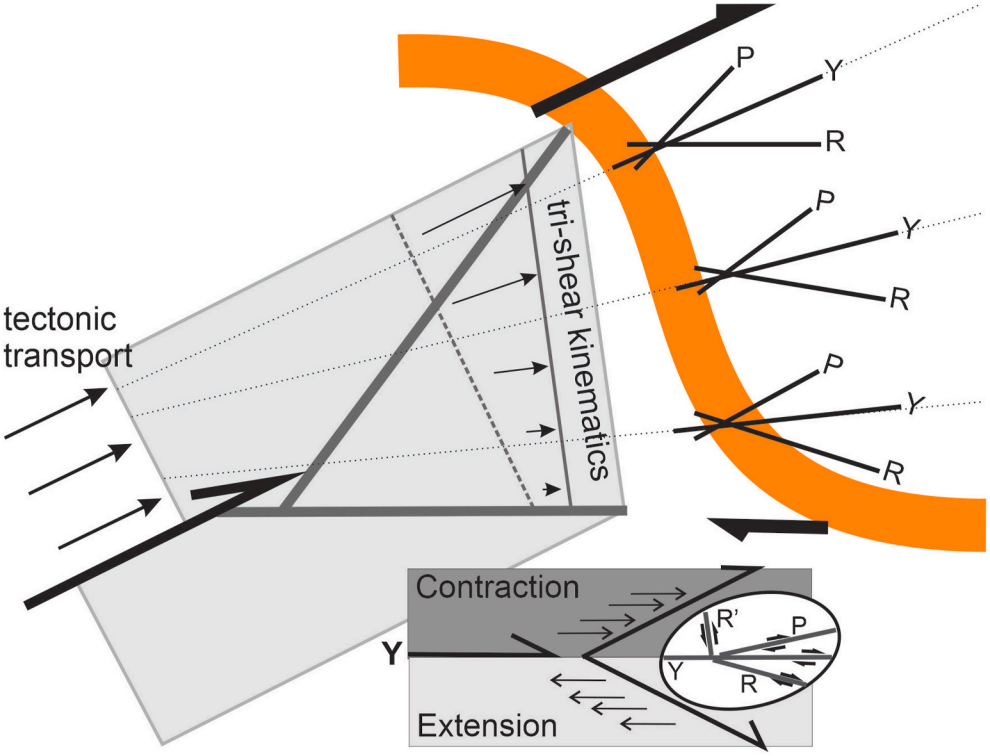

Fig. 12. Tri-shear fault-propagation fold model (inspired by Erslev 1991) for formation of monocline. During growth of deformation band swarms within the monocline, structures my experience a change from shear compaction (R) or isochoric (Y) bands into shear-dilation structures (R; bands or fractures). The displacement field places generated structures into contractional and extensional sectors depending on their orientation. P-structures form close to the boundary between volumetric contraction and extension sectors as defined by the Y-shear plane of isochoric strain. During progressive folding, structural swarms rotate and may hence transgress from one sector to the other as they develop. Complimentary influence on the deformation style comes from gentle fanning of the displacement vectors as predicted by the tri-shear model, reflecting growth of the fold by hinge migration that extends the monocline limb. This drives dilation that is more prominent in outer extents of the tri-shear zone.

progressively larger displacement upwards which, in the studied case, could prompt near-horizontal shear systems for a given stage during folding, irrespective of orientation of bedding. In addition, or complementary, (2) flexural slip related strain utilizing local interfaces in the stratigraphy, (3) outer arch extension during folding, maybe in combination with (3) inner arch contraction in the syncline bounding the base of the larger monocline, could add structural complexity.

Kinematics of small-scale structures compared to the strongly east-verging San Rafael Swell monocline can support the examination of the overall controls on deformation. Both antithetic and synthetic slip events are present; Populations 1 and 3 structures show west-directed shear, Population 2 east-directed shear, and Population 4 records NW-SE shortening and NE-SW extension, the latter oblique to the larger monocline. For Population 1, recording early layer-parallel shortening with consistent antithetic, west-directed shear direction throughout the Navajo Sandstone, there could perhaps be an abutting obstacle in the east, forcing counter-shear and thickening in layers. Alternatively, inner arch forcing near a syncline may be present even at a very early stage of folding, consistent with numerous out-of-the-syncline thrusts in the Carmel Formation. Population 2 can be explained as the formation of forward-directed discrete shear structures while upper parts of the monocline moved forward compared to lower parts during bed rotation, conforming to the vector field forecasted by a tri-shear model. For Population 3, deformation may be associated with recessive shear controlled by the frontal syncline, consistent with out-of-the-syncline shear structures which, as mentioned, are common in Laramide monoclines, and observed along the San Rafael Swell monoclinal limb (e.g., Brown 1994; Ferill et al., 2016). Population 4 of sub-vertical, conjugate shear structures records a shift in the principal stresses, consistent with near-horizontal NW-SE shortening and NE-SW extension. A similar shortening axis for this area was identified by Fischer and Christensen (2004) based in shear-fractures of the Carmel Formation (overlying the Navajo Sandstone and the Temple Cap Formation, Fig. 3A). They document that the tectonic transport axis varied systematically from north to south, in a gradual clockwise rotation. For the Uneva Mine Canyon, with the Population 4 shortening axis oblique to the overall approximately E-W shortening axis of the San Rafael Swell monocline, there is overall stretching by oblique-lateral escape along the monocline. We propose that the central region of the San Rafael Swell monocline propagated further eastward from larger fault offset (or slip to propagation ratio) on the underlying, controlling reverse fault. Thereby, the study area, which is south of the centre point, experienced late oblique kinematics.

6.1.1. Evolution of deformation bands versus fractures

Each population of small-scale structures records deformation characteristics of the local strain field, which expectedly evolves during folding. There could perhaps be changes in material properties over time with compaction and cementation, or as parts of layers are uplifted relative to other parts during km-amplitude folding. There could also be impact of local changes in bed rheology, for instance controlled by grain size distribution, grain bonding by cement or dissolution during diagenesis, or influence by fluid pressure (e.g., Torabi and Fossen 2009). For instance, repeated reactive fluid expulsion events signify dynamic fracture pressures (Sundal et al., 2016, 2017).

The detailed dataset of deformation bands and fractures can be subdivided into three assemblages of distinct deformation styles, in a gross sense showing increased influence of dilation with time, and coinciding with localization of deformation as illustrated in Fig. 11:

(1) Population 1 structures are deformation bands, which span from dominantly shear-compaction (P-bands) to shear-isochoric (Y) and subordinate shear-dilation (mild dilation; R) type bands.
(2) Populations 2 and 3 structures cover both deformation bands and fractures. Bands are shear-compaction (P and Y) to subordinate shear-isochoric (R). In larger offset (<50 cm) band swarms, bands can be seen to host and partly transform into shear fractures, appearing as cm-scale isolated patches or as dm-long partly connected fracture systems. Bands and fractures show similar shear-direction.
(3) Population 4 structures show mainly shear-dilation disaggregation deformation bands with sporadic mild cataclasis in cemented patches. These bands are directly linked to fractures with a high dilation to shear ratio, the latter of which makes up the continuation at the tip of bands or split mildly cataclastic bands. Bands and fractures record similar shear-direction.

A key observation is the variability in kinematics and deformation mechanism of deformation bands in uniform populations that appear concurrent. We advocate that deformation band formation, deformation band characteristics and fracturing are closely linked.

For Population 1, lamination and bedding guide locations of deformation bands. With R-bands following lamination in inter-dune facies, and with Y and P-bands cutting up across lamination with top-west offset, the strain is that of parallel or low-angle to bedding shear. Variations in orientation of lamination in foresets of compound dunes challenge a more specific analysis. Width and intensity of cataclasis seem to vary between band sets, with narrow P-bands offering more extensive cataclasis and porosity loss (Fig. 6), relative to R and Y bands. Y-bands are overall closer to isochoric, representing a transition to isochoric or mildly dilational, wider R-bands. As bands merge and splay, all three sets are closely linked in what is interpreted as a synchronously, unified shear system.

The observations above suggest there is a relationship between the orientation of bands and the degree of cataclasis and compaction, which is proposed to reflect their orientation within sectors of shortening and extension in a strain field (Fig. 12), conforming to Aydin et al.'s (2006; their Fig. 5b) comment of changing kinematics with band orientations. Consequently, minor differences in enveloping stresses on grain contacts for bands of various orientations play a role in the degree of grain breakage.

Population 2 and partly Population 3 structures offer a possible variation in cataclasis and compaction similar to Population 1. However, this is less well developed in Populations 2 and 3. Interaction of bands and fractures, as shown in Figs. 7 and 8, are suggested by slip-patches within deformation bands swarms in an overall coherent kinematic shear system, suggesting they are temporally linked. In these cases, fractures are hosted by bands; hence bands appear to predate fracturing. This observation conforms to that of Zuluaga et al. (2014), advocating for bands predating slip-surfaces. With fractures hosted by bands, compaction/cataclasis seems a pre-requisite for fracture formation, conforming to general observations that bands form in highly porous rocks and may be replaced by fractures following loss of porosity and related strain hardening, as a precursor to faulting (e.g., Davatzes and Aydin 2003; Fossen et al., 2007). The observation of transitions from deformation band to fracture in Population 2 is unique, as it expands on observations of slipped deformation bands (Rotevatn et al., 2008; Skurtveit et al., 2016; Braathen et al., 2018) and deviates from the general observation that bands pre-date fracturing during fault growth (Davatzes and Aydin 2003; Skurtveit et al., 2016). Perhaps the key to this transition in the deformation mechanism is the rotation of the developing shear structures in Population 2. As the deformation band swarm rotates during progressive folding, the orientation shifts alignment from the contractional to the extensional strain fields. In a rotation scenario, a developing shear-compaction deformation band swarm transgresses into shear-dilation, to a setting in which shear-failure is favoured.

The previous scenario is viable for Population 2. However, for Population 3; structures of top-west antithetic shear, overall fold-rotation would move active shear structures towards increased compaction. In this case, shear-fracture formation may be linked to slight dilation or isochoric shear on R-bands combined with gentle vertical dilation

caused by lengthening of the monocline fold-limb as forecasted by a trishear model.

In an extensional setting, annulled of compaction, disaggregation bands form, as especially well expressed by Population 4 structures. Occurrences of shear-dilation disaggregation deformation bands do display, however, sporadic mild cataclasis in cemented patches, pointing to impacts of grain-bonding cement towards a favoured deformation mechanism. This is an observation forwarded in several accounts (e.g., Skurtveit et al., 2016; Braathen et al., 2018). With band-tips linked to fractures that make up the continuation of a uniform shear system, bands and fractures appear synchronous. Further, examples of bands that have opened into patches of highly dilational shear fractures by loss of grain contacts illustrate how bands may evolve into "changeover" fractures (opening-mode discrete structures without cohesion) by significant dilation.

Of importance to the deformation mechanisms encountered for Population 4 are widespread calcite and oxide cements filling these deformation bands and fractures. Sundal et al. (2016) advocate that significant, high P, T fluid fracture flow and expulsion happened at this stage, as required for precipitating significant quantities of secondary minerals, filling fractures and forming rims of precipitate around relict reactive plumes. In light of the disaggregation deformation bands and fractures of Population 4, high fluid pressure would augment lower stress on grain contacts, promoting granular flow as the predominant deformation mechanism. High fluid pressure, approaching the lithostatic pressure and thereby weakening the sandstone, conforms to the observation of a very narrow bisector between the conjugate sets of structures with opposite kinematics in Population 4.

The above discussion on progressive deformation challenges the general view that deformation bands are irreplaceable, unique deformation products in sandstone. We advocate that deformation in highly porous sandstones, given conditions in a progressive shear system, causes revival of deformation bands by united band-fracture shear systems, expanding on Davatzes and Aydin (2003). Further, in situations of shear-dilation, deformation bands may directly progress into open fractures as grain contacts are departed.

7. Conclusions

Our investigation of deformation structures in the Navajo Sandstone in the Uneva Mine Canyon, a prime locality which cross-cuts the km-scale Laramide-style monocline of the San Rafael Swell (Utah, USA), shows:

1) Four Populations of small-scale structures record a progressive evolution of the first-order monocline.
2) Within the east-verging monocline, Populations 1 and 3 structures are west-directed, Population 2 east-directed, and Population 4 records NW-SE shortening and NE-SW extension that is oblique to the regional monocline.
3) The Populations record three different assemblages of structures; initial shear-compaction deformation bands, followed by shear-compaction band swarms that host fractures, and finally shear-dilation disaggregation deformation bands formed in union with fractures. The latter links to elevated fluid pressure weakening the Navajo Sandstone.
4) Kinematics and deformation mechanisms support progressive formation of deformation bands and fractures during growth of the major monocline. Interactions of deformation bands and fractures suggest transitions of deformation bands into mutual shear band and fracture systems.
5) For four successive Populations of deformation bands, orientation of individual bands versus deformation mechanism suggest impact of contractional and extensional strain sectors in a shear system.

Declaration of competing interest

The authors declare that they have no known competing financial interests or personal relationships that could have appeared to influence the work reported in this paper.

Acknowledgements

This research was undertaken as part of the COPASS and COTEC projects, and the NCCS Centre, funded by the Research Council of Norway under grants # 244049, 295061 and 257579. Contributions by the University of Oslo, Western State Colorado University and Colorado School of Mines are acknowledged. Braathen thank the German University of Technology in Oman (GUtech) for hosting him and offering a stimulating work environment during the writing of this article.

References

Ahlgren, S.G., 2001. The nucleation and evolution of Riedel shear zones as deformation bands in porous sandstone. J. Struct. Geol. 23 (8), 1203–1214.
Allmendinger, R.W., 1998. Inverse and forward numerical modeling of trishear fault-propagation folds. Tectonics 17 (4), 640–656.
Averitt, P., Detterman, J.S., Harshbarger, J.W., Repenning, C.A., Wilson, R.F., 1955. Revisions in correlation and nomenclature of Triassic and Jurassic formations in southwestern Utah and northern Arizona. AAPG (Am. Assoc. Pet. Geol.) Bull. 39, 2515–2535.
Aydin, A., 1978. Small faults formed as deformation bands in sandstone. In: Rock Friction and Earthquake Prediction. Birkhäuser, Basel, pp. 913–930.
Aydin, A., Ahmadov, R., 2009. Bed-parallel compaction bands in eolian sandstone: their identification, characterization and implications. Tectonophysics 479 (3–4), 277–284.
Aydin, A., Johnson, A.M., 1978. Development of faults as zones of deformation bands and as slip surfaces in sandstone. Pure Appl. Geophys. 116 (4–5), 931–942.
Aydin, A., Johnson, A.M., 1983. Analysis of faulting in porous sandstones. J. Struct. Geol. 5 (1), 19–31.
Aydin, A., Borja, R.I., Eichhubl, P., 2006. Geological and mathematical framework for failure modes in granular rock. J. Struct. Geol. 28 (1), 83–98.
Ballas, G., Soliva, R., Sizun, J.P., Benedicto, A., Cavailhes, T., Raynaud, S., 2012. The importance of the degree of cataclasis in shear bands for fluid flow in porous sandstone, Provence, France. AAPG (Am. Assoc. Pet. Geol.) Bull. 96 (11), 2167–2186.
Ballas, G., Soliva, R., Sizun, J.P., Fossen, H., Benedicto, A., Skurtveit, E., 2013. Shear-enhanced compaction bands formed at shallow burial conditions; implications for fluid flow (Provence, France). J. Struct. Geol. 47, 3–15.
Ballas, G., Fossen, H., Soliva, R., 2015. Factors controlling permeability of cataclastic deformation bands and faults in porous sandstone reservoirs. J. Struct. Geol. 76, 1–21.
Berg, S.S., Skar, T., 2005. Controls on damage zone asymmetry of a normal fault zone: outcrop analyses of a segment of the Moab fault, SE Utah. J. Struct. Geol. 27 (10), 1803–1822.
Bergbauer, S., Pollard, D.D., 2004. A new conceptual fold-fracture model including prefolding joints, based on the Emigrant Gap anticline, Wyoming. Geol. Soc. Am. Bull. 116 (3–4), 294–307.
Bird, P., 1998. Kinematic history of the Laramide orogeny in latitudes 35–49 N, western United States. Tectonics 17 (5), 780–801.
Braathen, A., Tveranger, J., Fossen, H., Skar, T., Cardozo, N., Semshaug, S.E., Bastesen, E., Sverdrup, E., 2009. Fault facies and its application to sandstone reservoirs. AAPG (Am. Assoc. Pet. Geol.) Bull. 93 (7), 891–917.
Braathen, A., Osmundsen, P.T., Hauso, H., Semshaug, S., Fredman, N., Buckley, S.J., 2013. Fault-induced deformation in a poorly consolidated, siliciclastic growth basin: a study from the Devonian in Norway. Tectonophysics 586, 112–129.
Braathen, A., Midtkandal, I., Mulrooney, M.J., Appleyard, T.R., Haile, B.G., van Yperen, A.E., 2018. Growth-faults from delta collapse–structural and sedimentological investigation of the Last Chance delta, Ferron Sandstone, Utah. Basin Res. 30 (4), 688–707.
Brandenburg, J.P., Alpak, F.O., Solum, J.G., Naruk, S.J., 2012. A kinematic trishear model to predict deformation bands in a fault-propagation fold, East Kaibab monocline, Utah. AAPG (Am. Assoc. Pet. Geol.) Bull. 96 (1), 109–132.
Bromley, M., 1992. Topographic inversion of early interdune deposits, Navajo sandstone (lower jurassic), Colorado plateau, USA. Sediment. Geol. 80 (1–2), 1–25.
Brown, W.G., 1993. Structural style of Laramide basement-cored uplifts and associated folds. Geology of Wyoming: Geological Survey of Wyoming Memoir 5, 312–371.
Cardozo, N., Jackson, C.A.L., Whipp, P.S., 2011. Determining the uniqueness of best-fit trishear models. J. Struct. Geol. 33 (6), 1063–1078.
Cashman, S., Cashman, K., 2000. Cataclasis and deformation-band formation in unconsolidated marine terrace sand, Humboldt County, California. Geology 28 (2), 111–114.
Cooper, S.P., Goodwin, L.B., Lorenz, J.C., 2006. Fracture and fault patterns associated with basement-cored anticlines: the example of Teapot Dome, Wyoming. AAPG (Am. Assoc. Pet. Geol.) Bull. 90 (12), 1903–1920.

Davatzes, N.C., Aydin, A., 2003. Overprinting faulting mechanisms in high porosity sandstones of SE Utah. J. Struct. Geol. 25 (11), 1795–1813.
Davis, G.H., 1999. Structural geology of the Colorado Plateau region of southern Utah, with special emphasis on deformation bands. Geological Society of America 342.
Doelling, H.H., 2001. Geologic map of the moab and eastern part of the san rafael desert 30' x 60' quadrangles, grand and emery counties, Utah, and Mesa county, Colorado. Utah Geological Survey Map 180, 3 plates, scale 1:100,000.
Doelling, H.H., Sprinkel, D.A., Kowallis, B.J., Kuehne, P.A., 2013. Temple Cap and Carmel formations in the Henry mountains basin, Wayne and garfield counties, Utah. In: The San Rafael Swell and Henry Mountains Basin—geologic Centerpiece of Utah, vol. 42. Utah Geological Association Publication, pp. 279–318.
Doelling, H.H., Kuehne, P.A., Willis, G.C., Ehler, J.B., 2015. Geologic map of the san rafael desert 30' x 60' quadrangle, emery and grand counties, Utah. Utah Geological Survey, Map 267DM, scale 1 62, 500.
Dresen, G., 1991. Stress distribution and the orientation of Riedel shears. Tectonophysics 188 (3–4), 239–247.
EolCardozo, N., Aanonsen, S., 2009. Optimized trishear inverse modeling. J. Struct. Geol. 31 (6), 546–560.
Erslev, E.A., 1991. Trishear fault-propagation folding. Geology 19 (6), 617–620.
Ferrill, D.A., Morris, A.P., Wigginton, S.S., Smart, K.J., McGinnis, R.N., Lehrmann, D., 2016. Deciphering thrust fault nucleation and propagation and the importance of footwall synclines. J. Struct. Geol. 85, 1–11.
Fischer, M.P., Christensen, R.D., 2004. Insights into the growth of basement uplifts deduced from a study of fracture systems in the San Rafael monocline, east central Utah. Tectonics 23 (1).
Fossen, H., 2010. Deformation bands formed during soft-sediment deformation: observations from SE Utah. Mar. Petrol. Geol. 27 (1), 215–222.
Fossen, H., Schultz, R.A., Shipton, Z.K., Mair, K., 2007. Deformation bands in sandstone: a review. J. Geol. Soc. 164 (4), 755–769.
Fossen, H., Zuluaga, L.F., Ballas, G., Soliva, R., Rotevatn, A., 2015. Contractional deformation of porous sandstone: insights from the aztec sandstone, SE Nevada, USA. J. Struct. Geol. 74, 172–184.
Hancock, P.L., 1985. Brittle microtectonics: principles and practice. J. Struct. Geol. 7 (3–4), 437–457.
Harshbarger, J.W., Repenning, C.A., Irwin, J.H., 1957. Stratigraphy of the uppermost Triassic and the Jurassic rocks of the Navajo country. U. S. Geol. Surv. Prof. Pap. 291, 74.
Hassan, M.S., Venetikidis, A., Bryant, G., Miall, A.D., 2018. The sedimentology of an ERG margin: the Kayenta–Navajo transition (lower jurassic), Kanab, Utah, USA. J. Sediment. Res. 88 (5), 613–640. https://doi.org/10.2110/jsr.2018.31.
Havholm, K.G., Kocurek, G., 1994. Factors controlling eolian sequence stratigraphy: clues from super bounding surface features in the Middle Jurassic Page Sandstone. Sedimentology 41 (5), 913–934. https://doi.org/10.1111/j.1365-3091.1994.tb01432.x.
Hintze, L.F., 1980. Geologic map of Utah. Utah Geol. Mineral. Surv., scale 1, 500,000.
Hintze, L., Kowallis, B., 2009. Geological History of Utah. Brigham Young University Geology Studies.
Ismat, Z., Mitra, G., 2005. Folding by cataclastic flow: evolution of controlling factors during deformation. J. Struct. Geol. 27 (12), 2181–2203.
Kocurek, G., 1988. First-order and super bounding surfaces in eolian sequences—bounding surfaces revisited. Sediment. Geol. 56 (1–4), 193–206.
Middleton, L.T., Blakey, R.C., 1983. Processes and controls on the intertonguing of the Kayenta and Navajo formations, northern Arizona: eolian–fluvial interactions. In: Brookfield, M.E., Ahlbrandt, T.S. (Eds.), Eolian Sediments and Processes: Amsterdam, vol. 38. Elsevier, pp. 613–634. Developments in Sedimentology.
Misra, S., Mandal, N., Chakraborty, C., 2009. Formation of Riedel shear fractures in granular materials: Findings from analogue shear experiments and theoretical analyses. Tectonophysics 471 (3–4), 253–259.
Petit, J.P., 1987. Criteria for the sense of movement on fault surfaces in brittle rocks. J. Struct. Geol. 9 (5–6), 597–608.
Petrie, E.S., Sundal, A., Gutierrez, M., Braathen, A., 2017. Deformation band formation and reactivation associated with a Laramide fault propagation fold. Geological Society of America Abstract with Programs 49, 289–299.
Pizzati, M., Balsamo, F., and Storti, F., (in press). Displacement-dependent microstructural and petrophysical properties of deformation bands and gouges in poorly lithified sandstone deformed at shallow burial depth (Crotone Basin, Italy). J. Struct. Geol., 104069.
Pizzati, M., Balsamo, F., Storti, F., Iacumin, P., 2020. Physical and chemical strain-hardening during faulting in poorly lithified sandstone: the role of kinematic stress field and selective cementation. Geol. Soc. Am. Bull. 132 (5–6), 1183–1200.
Priddy, C.L., Clarke, S.M., 2020. The sedimentology of an ephemeral fluvial–eolian succession. Sedimentology 1–34.
Riedel, W., 1929. Zur Mechanik geologischer Brucherscheinungen ein Beitrag zum Problem der Fiederspatten. Zentbl. Miner. Geol. Palaont. Abt. 354–368.
Rotevatn, A., Torabi, A., Fossen, H., Braathen, A., 2008. Slipped deformation bands: a new type of cataclastic deformation bands in Western Sinai, Suez rift, Egypt. J. Struct. Geol. 30 (11), 1317–1331.
Schueller, S., Braathen, A., Fossen, H., Tveranger, J., 2013. Spatial distribution of deformation bands in damage zones of extensional faults in porous sandstones: statistical analysis of field data. J. Struct. Geol. 52, 148–162.
Schultz, R.A., Balsko, C.M., 2003. Growth of deformation bands into echelon and ladder geometries. Geophysical Research Letters 30 (20).
Schultz, R.A., Fossen, H., 2008. Terminology for structural discontinuities. AAPG (Am. Assoc. Pet. Geol.) Bull. 92 (7), 853–867.
Shipton, Z.K., Cowie, P.A., 2001. Damage zone and slip-surface evolution over μm to km scales in high-porosity Navajo sandstone, Utah. J. Struct. Geol. 23 (12), 1825–1844.
Shipton, Z.K., Evans, J.P., Robeson, K.R., Forster, C.B., Snelgrove, S., 2002. Structural heterogeneity and permeability in faulted eolian sandstone: implications for subsurface modeling of faults. AAPG (Am. Assoc. Pet. Geol.) Bull. 86 (5), 863–883.
Silliphant, L.J., Engelder, T., Gross, M.R., 2002. The state of stress in the limb of the Split Mountain anticline, Utah: constraints placed by transected joints. J. Struct. Geol. 24 (1), 155–172.
Skurtveit, E., Torabi, A., Gabrielsen, R.H., Zoback, M.D., 2013. Experimental investigation of deformation mechanisms during shear-enhanced compaction in poorly lithified sandstone and sand. J. Geophys. Res.: Solid Earth 118 (8), 4083–4100.
Skurtveit, E., Torabi, A., Alikarami, R., Braathen, A., 2015. Fault baffle to conduit developments: reactivation and calcite cementation of deformation band fault in eolian sandstone. Petrol. Geosci. 21 (1), 3–16.
Skurtveit, E., Braathen, A., Larsen, E.B., Sauvin, G., Sundal, A., Zuchuat, V., 2017. Pressure induced deformation and flow using CO2 field analogues, Utah. Energy Procedia 114, 3257–3266.
Soliva, R., Schultz, R.A., Ballas, G., Taboada, A., Wibberley, C., Saillet, E., Benedicto, A., 2013. A model of strain localization in porous sandstone as a function of tectonic setting, burial and material properties; new insight from Provence (southern France). J. Struct. Geol. 49, 50–63.
Solum, J.G., Davatzes, N.C., Lockner, D.A., 2010. Fault-related clay authigenesis along the Moab Fault: implications for calculations of fault rock composition and mechanical and hydrologic fault zone properties. J. Struct. Geol. 32 (12), 1899–1911.
Sprinkel, D.A., Doelling, H.H., Kowallis, B.J., Waanders, G., Kuehne, P.A., Yonkee, W.A., Chidsey, T.C., 2011. Early results of a study of Middle Jurassic strata in the Sevier fold and thrust belt, Utah. In: Sevier Thrust Belt: Northern and Central Utah and Adjacent Areas, vol. 40. Utah Geological Association, Publication, pp. 151–172.
Sundal, A., Petrie, E., Hellevang, H., Midtkandal, I., Braathen, A., 2016. Reactive fluid expulsion during progressive deformation in the fold limb of the san rafael swell, Utah, USA. In: GSA Annual Meeting in Denver, Colorado, USA. Session No. 171, 26.09.2016, T212. Multifaceted Approaches to Understanding Fluid-Fault Interactions in Natural Resources and Geologic Hazards (Posters).
Sundal, A., Miri, R., Hellevang, H., Tveranger, J., Midtkandal, I., Zuchuat, V., Aagaard, P., Braathen, A., 2017. Movement of CO_2 charged fluids in low permeability rocks during deformation: migration patterns in the Carmel Formation, Utah. Energy Procedia 114, 4537–4544.
Torabi, A., Fossen, H., 2009. Spatial variation of microstructure and petrophysical properties along deformation bands in reservoir sandstones. AAPG (Am. Assoc. Pet. Geol.) Bull. 93 (7), 919–938.
Tueckmantel, C., Fisher, Q.J., Knipe, R.J., Lickorish, H., Khalil, S.M., 2010. Fault seal prediction of seismic-scale normal faults in porous sandstone: a case study from the eastern Gulf of Suez rift, Egypt. Mar. Petrol. Geol. 27 (2), 334–350.
Wibberley, C.A., Yielding, G., Di Toro, G., 2008. Recent advances in the understanding of fault zone internal structure: a review. Geological Society, London, Special Publications 299 (1), 5–33.
Witkind, I.J., 1988. Geologic Map of the Huntington 30′ X 60′ Quadrangle, Carbon, Emery, Grand, and Uintah Counties. Utah.
Yonkee, W.A., Weil, A.B., 2015. Tectonic evolution of the sevier and Laramide belts within the north American cordillera orogenic system. Earth Sci. Rev. 150, 531–593.
Zuchuat, V., Sleveland, A., Sprinkel, D., Rimkus, A., Braathen, A., Midtkandal, I., 2018. New insights on the impact of tidal currents on a low-gradient, semi-enclosed, epicontinental basin—the Curtis Formation, east-central Utah, USA. Geology of the Intermountain West 5, 131–165.
Zuchuat, V., Sleveland, A.R., Pettigrew, R.P., Dodd, T.J., Clarke, S.M., Rabbel, O., Braathen, A., Midtkandal, I., 2019a. Overprinted allocyclic processes by tidal resonance in an epicontinental basin: the Upper Jurassic Curtis Formation, east-central Utah, USA. The Depositional Record 5, 272–305.
Zuchuat, V., Midtkandal, I., Poyatos-Moré, M., Da Costa, S., Brooks, H.L., Halvorsen, K., Braathen, A., 2019b. Composite and diachronous stratigraphic surfaces in low-gradient, transitional settings: the J-3 "unconformity" and the Curtis Formation, east-central Utah, USA. J. Sediment. Res. 89 (11), 1075–1095.
Zuluaga, L.F., Fossen, H., Rotevatn, A., 2014. Progressive evolution of deformation band Populations during Laramide fault-propagation folding: Navajo Sandstone, San Rafael monocline, Utah, USA. J. Struct. Geol. 68, 66–81.